

A dormant, overmassive black hole in the early Universe

Ignas Juodžbalis^{1,2*}, Roberto Maiolino^{2,3†}, William M. Baker^{1,2†},
Sandro Tacchella^{1,2†}, Jan Scholtz^{1,2†}, Francesco D'Eugenio^{1,2†},
Raffaella Schneider^{3,4,5,6†}, Alessandro Trinca^{3,4,5†},
Rosa Valiante^{4,5†}, Christa DeCoursey^{7†}, Mirko Curti⁸,
Stefano Carniani⁹, Jacopo Chevallard¹⁰, Anna de Graaff¹¹,
Santiago Arribas¹², Jake S. Bennett¹³, Martin A. Bourne^{1, 14},
Andrew J. Bunker¹⁰, Stéphane Charlot¹⁵, Brian Jiang¹,
Sophie Koudmani^{1, 14, 15, 16}, Michele Perna¹², Brant Robertson¹⁸,
Debora Sijacki^{1, 14}, Hannah Übler^{1,2}, Christina C. Williams¹⁹,
Chris Willott²⁰, Joris Witstok^{1, 2†}

¹Kavli Institute for Cosmology, University of Cambridge, Madingley Road, Cambridge, CB3 0HA, UK.

²Cavendish Laboratory - Astrophysics Group, University of Cambridge, 19 JJ Thomson Avenue, Cambridge, CB3 0HE, UK.

³Dipartimento di Fisica, “Sapienza” Università di Roma, Piazzale Aldo Moro 2, Roma, 00185, Italy.

⁴Osservatorio Astronomico di Roma, INAF, Via di Frascati 33, Monte Porzio Catone, 00040, Italy.

⁵INFN, Sezione Roma1, “Sapienza” Università di Roma, Piazzale Aldo Moro 2, Roma, 00185, Italy.

⁶Sapienza School for Advanced Studies, Viale Regina Elena 291, Roma, 00161, Italy.

⁷Steward Observatory, University of Arizona, 933 N. Cherry Avenue, Tucson, 85721, Arizona USA.

⁸European Southern Observatory, Karl-Schwarzschild-Strasse 2, Garching, D-85748, Germany.

⁹Scuola Normale Superiore, Piazza dei Cavalieri 7, Pisa, I-56126, Italy.

¹⁰Department of Physics, University of Oxford, Denys Wilkinson Building, Keble Road, Oxford, OX1 3RH, UK.

- ¹¹Max-Planck-Institut für Astronomie, Königstuhl 17, Heidelberg, D-69117, Germany.
- ¹²Centro de Astrobiología (CAB), CSIC-INTA, Cra. de Ajalvir Km. 4, Torrejón de Ardoz, Madrid, 28850, Spain.
- ¹³Center for Astrophysics, Harvard University, 60 Garden Street, Cambridge, 02138, Massachusetts, USA.
- ¹⁴Institute of Astronomy, University of Cambridge, Madingley Road, Cambridge, CB3 0HA, UK.
- ¹⁵Institut d'Astrophysique de Paris, Sorbonne Université, CNRS, UMR 7095, 98 bis bd Arago, Paris, F-75014, France.
- ¹⁶St Catharine's College, University of Cambridge, Trumpington Street, Cambridge, CB2 1RL, UK.
- ¹⁷Center for Computational Astrophysics, Flatiron Institute, 162 5th Avenue, New York, 10010, USA.
- ¹⁸Department of Astronomy and Astrophysics, University of California, 1156 High Street, Santa Cruz, 96054, California, USA.
- ¹⁹NSF's National Optical-Infrared Astronomy Research Laboratory, 950 North Cherry Avenue, Tucson, 85719, Arizona USA.
- ²⁰NRC Herzberg, 5071 West Saanich Rd, Victoria, BC V9E 2E7, Canada.

*Corresponding author(s). E-mail(s): ij284@cam.ac.uk;

†These authors contributed equally to this work.

Abstract

Recent observations have found a large number of supermassive black holes already in place in the first few hundred million years after Big Bang [1–10]. The channels of formation and growth of these early, massive black holes are not clear, with scenarios ranging from heavy seeds to light seeds experiencing bursts of high accretion rate [11–17]. Here we present the detection, from the JADES survey, of broad H α emission in a galaxy at $z=6.68$, which traces a black hole with mass of $\sim 4 \times 10^8 M_{\odot}$ and accreting at a rate of only 0.02 times the Eddington limit. The host galaxy has low star formation rate ($\sim 1 M_{\odot}/yr$, a factor of 3 below the star forming main sequence). The black hole to stellar mass ratio is ~ 0.4 , i.e. about 1,000 times above the local relation, while the system is closer to the local relations in terms of dynamical mass and velocity dispersion of the host galaxy. This object is most likely the tip of the iceberg of a much larger population of dormant black holes around the epoch of reionisation. Its properties are consistent with scenarios in which short bursts of super-Eddington accretion have resulted in black hole overgrowth and massive gas expulsion from the accretion disk; in between bursts, black holes spend most of their life in a dormant state.

Keywords: Black Holes, Active Galactic Nuclei, Super-Eddington accretion, Galaxy Evolution

The galaxy JADES GN+189.09144+62.22811 1146115, located in the GOODS-N field (R.A. = 189° 5′ 29.2″, Dec = 62° 13′ 41.2″), was observed with JWST both with NIRCam and with the NIRSpec multi-object mode, both with the low resolution prism and medium resolution gratings as part of the JADES (JWST Advanced Extragalactic Survey), PID:1181. The NIRSpec spectra reveal multiple emission nebular lines (Extended Data Figure 5), which unambiguously show that the galaxy is at $z = 6.677$.

The $H\alpha$ line is in the gap of the medium resolution grating spectrum and observed only in the prism spectrum Figure 1. However, the resolution at this wavelength ($R \sim 460$ for a compact source) is sufficient to reveal a clear broad component of this line. The broad component is fairly symmetric and not seen in [OIII] (whose narrow component is stronger than $H\alpha$, see Methods and Extended Data Figure 9). This suggests that the broad $H\alpha$ line is not associated with outflows, leaving as the most plausible interpretation the Broad Line Region (BLR) of an accreting black hole (BH), i.e. an Active Galactic Nucleus (AGN). We rule out the possibility that this broad-line component may be attributed to a supernova (SN), due to the lack of variability, or the effect of multiple SNe, given, as we will see, the moderate star formation rate (SFR) of the galaxy (see Methods for details).

We note that the spectrum shown in Figure 1 appears to have a feature at $\lambda \approx 4.94 \mu\text{m}$, the origin of which is currently unclear. Thus, we choose to mask it in the final fit, although its inclusion would not significantly affect the results. An extended discussion on the possible origin of this feature is presented in the Methods.

When fitted with two Gaussian components (see Methods), the broad component has a width (Full Width Half Maximum) of $5700_{-1100}^{+1700} \text{ km s}^{-1}$ and a flux of $27.3_{-4.0}^{+4.1} \times 10^{-19} \text{ erg s}^{-1} \text{ cm}^{-2}$. Assuming the local virial relations [18, 19], and taking into account the effect of some dust obscuration, we estimate a black hole mass of $\log M_{\text{BH}}/M_{\odot} = 8.61_{-0.24}^{+0.27}$, with a systematic scatter of 0.33 dex (see Methods for details).

Coupled with the bolometric luminosity, estimated from the broad component of $H\alpha$ (following the scaling relation given by [20]), but also consistently from the photometric fit of the nuclear component, we infer that the galaxy is accreting at 2.4% of its Eddington limit, i.e. $\lambda_{\text{Edd}} \equiv L_{\text{bol}}/L_{\text{Edd}} = 0.024_{-0.008}^{+0.011}$, with a systematic scatter of 0.5 dex (see Methods for details).

We note that a recent measurement of the black hole mass in a super-Eddington accreting quasar at $z \sim 2$ has cast doubts on the validity of the UV virial relations for single-epoch black hole measurements [21]. The same work, however, points out that when using $H\alpha$ to measure the black hole mass, the discrepancy is only a factor of 2.5. Moreover, the discrepancy has been ascribed to deviations of the BLR size in the super-Eddington regime, which is certainly not the case for JADES GN 1146115. In summary, the black hole mass measurement inferred from the broad $H\alpha$ in JADES GN 1146115 is reasonably solid.

Information on the host galaxy was obtained through multi-band NIRCam imaging. The fact that the AGN is so underluminous allows constraining the properties of the host galaxy much better than in luminous quasar. We employed the ForcePho tool to decompose the contribution of the nuclear region, hosting the unresolved AGN, from the host galaxy. Details on the morphological decomposition are provided in the

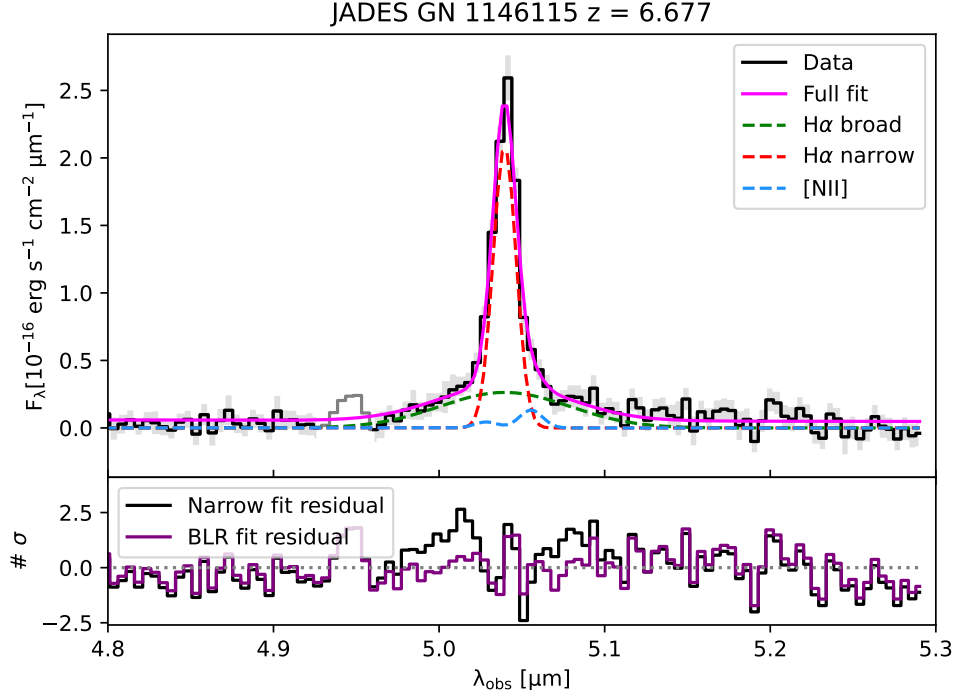


Fig. 1 Spectrum of JADES GN 1146115 around H α showing the presence of a broad component. **Top panel:** Observed spectrum (black solid line, with grey shading indicating 1σ uncertainties) along with the best fit line to the narrow (red dashed) and broad (green dashed) components. The [NII] doublet is shown in blue and it is only marginally detected at 2σ . The magenta solid line shows the total fit. The greyed line portion at $\sim 4.95 \mu\text{m}$ of the spectrum shows the region, which was masked due to a possible artefact or H α emission from a lower redshift interloper. **Bottom panel:** Fit residuals shown for a simple narrow H α and [NII] fit (black line) and the best-fit, containing a broad component (purple line). It can be seen that the narrow line only fit does not account for the broad wings of the line, leaving significant systematic residuals.

Methods section. Here we simply mention that the morphology can be well fitted with a nuclear unresolved source and a compact ($R_e \sim 140 \text{ pc}$) host galaxy with a disc-like profile (Sérsic index $n \sim 1$).

The 8 bands photometry of the host galaxy was then fitted with the Bayesian SED fitting codes `BAGPIPES` [22] and `Prospector` [23] (see Methods), assuming flexible, non-parametric, star-formation histories (SFH). These fits, averaged together, yield a stellar mass $\log(M_*/M_\odot) = 8.92^{+0.30}_{-0.31}$ and instantaneous star formation rate $\text{SFR} = 1.38^{+0.92}_{-0.45} M_\odot \text{ yr}^{-1}$.

The SFH, shown in the Methods section, are poorly constrained, but consistent between the codes and suggesting that the galaxy experienced almost constant star formation over the last few 100 Myr. A comparison of JADES GN 1146115 with the star forming main sequence at similar redshifts is shown in Figure 2. Our source lies

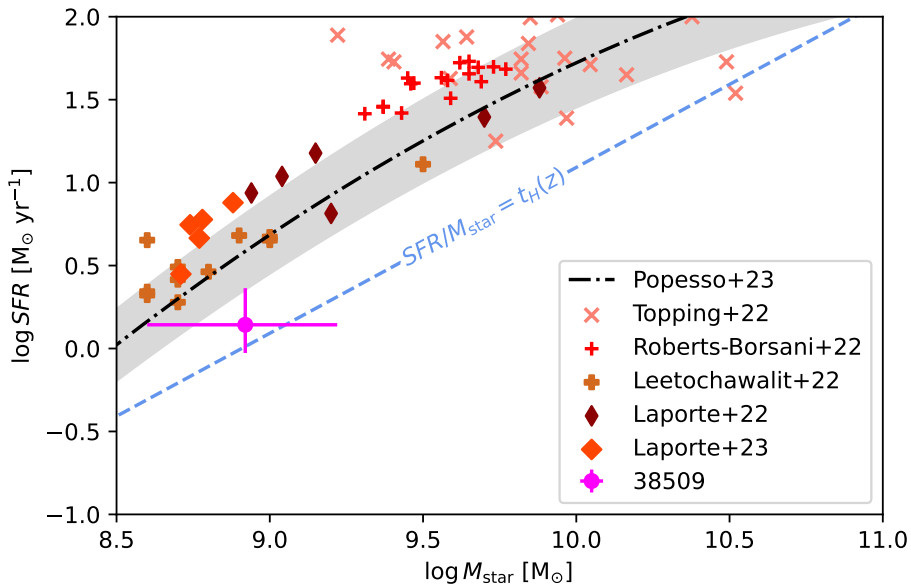


Fig. 2 Star-formation rate versus stellar mass diagram showing the location of JADES GN 1146115 with respect to the star forming main sequence. The black dash-dotted line shows the star forming main sequence fit from [24] extrapolated to $z = 6.677$, with the grey shaded area representing the uncertainties. Data at $7 < z < 9$ from [25–28] and [29] is shown with brown and red symbols. The dashed blue line indicates the limit below which it takes a galaxy more than the Hubble time at $z = 6.677$ to double its mass. The magenta circle shows the location of JADES GN 1146115, which is consistent with the dashed line within 1σ .

below the star-forming locus of similarly massive galaxies by a factor of ~ 3 , and would take ~ 1 Gyr (i.e. about the age of the Universe at $z \sim 6$) to double its mass with the current SFR. This indicates that the galaxy is currently fairly quiescent and may have been so for quite some time, although uncertainties on the SFH are large. The presence of AGN activity might offer a possible explanation for this state of the host, suggesting that AGN negative feedback might be responsible for suppressing star formation.

Figure 3 shows the location of JADES GN 1146115 (large magenta circle) on the L/L_{Edd} vs M_{BH} diagram (left panels) and on the M_{BH} vs M_{star} diagram (right panels). On the top panels, our source is compared with other AGN discovered by previous JWST studies at similar redshifts ($4 < z < 11$, blue symbols) [1–8, 30], along with bright $z > 5$ QSOs observed with JWST (orange/yellow symbols) [31–35]. The top-left panel illustrates that our object is among the most massive black holes found by JWST, with a mass similar to that of luminous high redshift quasars, but it accretes at a rate lower by about 2 orders of magnitude. Therefore, our object is the dormant counterpart of luminous, high redshift quasars.

Additionally, the top-right diagram indicates that our object is one of the most “overmassive” BHs found by JWST, in the sense that the BH mass approaches 50%

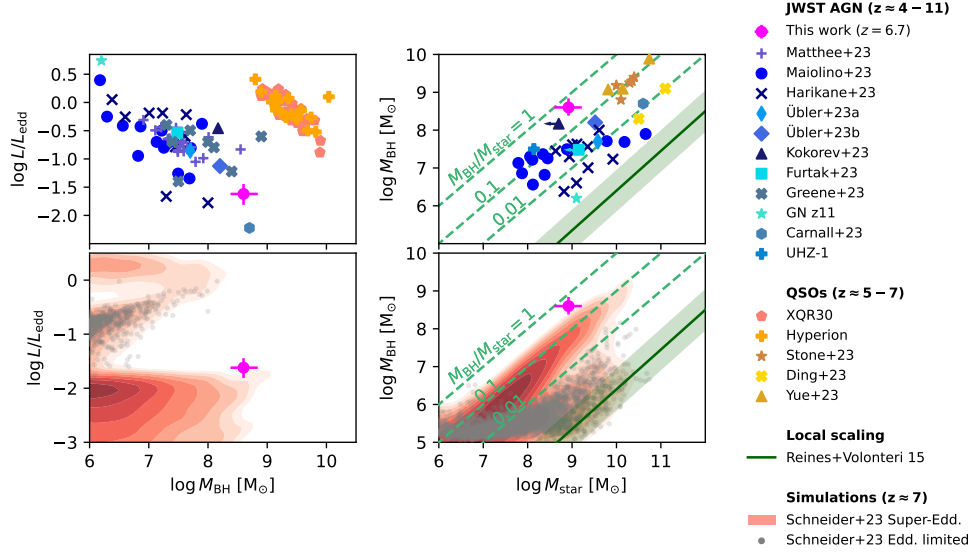


Fig. 3 Comparison of JADES GN 1146115 with other high- z AGN and models in terms of accretion rate, black hole mass and stellar mass of the host galaxy. **Left panels:** accretion rate relative to the Eddington limit, λ_{Edd} , versus black hole mass, $\log M_{\text{BH}}$. **Right panels:** Black hole mass versus stellar mass of the host galaxy $\log M_{\text{star}}$. Green dashed lines indicate constant $M_{\text{BH}}/M_{\text{star}}$ ratios, while the solid green line represents the local relation from [19], the shaded region shows the scatter. In all panels JADES GN 1146115 is indicated with a magenta circle and errorbars. **Top panels:** Comparison with other JWST-discovered AGN at high redshift (blue symbols [1–8, 30]) and with the QSO population at similar redshifts (orange/yellow symbols [31–35]). The observed negative correlation between λ_{Edd} and M_{BH} is likely reflective of Eddington luminosity’s dependence on black hole mass and observational incompleteness and not a separate physical phenomenon. **Bottom panels:** Comparison with the predictions (at $z \sim 7$) from the semi-analytical models from [11, 12] in the scenario of Eddington-limited accretion (grey points) and the scenario of light or heavy seeds that can experience super-Eddington accretion (red shaded contours).

of the host’s stellar mass, i.e. about 1,000 times above the local relation between BH and host galaxy stellar mass.

The JWST finding of several overmassive black holes at high redshift [1, 2, 4, 9, 36] has been interpreted by some works [37, 38] as the result of a large scatter of the BH-stellar mass relation combined with selection effects, in the sense that more massive black holes tend to be preferentially selected, as they can reach higher luminosities. While assessing biases in the offset of the BH-stellar mass relation at high redshift is beyond the scope of this paper, we note that our finding of such highly overmassive black hole associated with a low luminosity AGN, due to its low Eddington ratio, is incompatible with the selection effect scenarios. Specifically, the scenario proposed by [38] (which envisages a BH-stellar relation similar to the local one, but with an order of magnitude scatter) hardly reaches the BH-to-stellar mass ratio observed in our object, and their observational bias scenario would require an observed luminosity of $\sim 10^{45-46}$ erg/s, i.e. 2-3 dex above the luminosity observed in

JADES GN 1146115 prior to dust obscuration correction. The Trinity simulation [37] can produce overmassive black holes as observed in JADES GN 1146115, but they require even higher luminosities, in excess of 10^{48} erg/s, hence totally incompatible with the luminosity of our object. Therefore, while selection effects are important (as we will illustrate more thoroughly below), our finding suggests that the overmassive nature of high- z BHs is also associated with an intrinsic offset of the BH-stellar mass relation, as also suggested by other studies [14].

Some previous studies have found that early black holes are overmassive only relative to the stellar mass, but when compared with the velocity dispersion and dynamical mass of the host galaxy they are more aligned with the local relation ([2, 21]). This would indicate that the baryonic mass of the host galaxy is already in place, but that star formation is lagging behind, possibly due to feedback generated by black hole accretion. In the case of JADES GN 1146115, based on the profile of the [O III] doublet in the medium resolution spectrum, we derive a stellar velocity dispersion of $\sigma_* \approx 121$ km s $^{-1}$ and a dynamic mass to be on the order of $10^{9.5} M_\odot$ (see Methods for details). This would place JADES GN 1146115 ‘only’ 10 - 20 times above the local scaling relations derived by [39, 40], however, it remains marginally consistent with the empirical scatter on them as shown in Figure 15 in Methods. This suggests that the overmassive nature of JADES GN 1146115 (as for other high- z AGN) is primarily relative to the stellar mass of the host galaxy, while much closer to local relations when compared with the velocity dispersion and dynamical mass of the host.

The presence of overmassive black holes in the early Universe has been explained by a variety of models and cosmological simulations. These predict that either black holes are born from relatively massive seeds (e.g. direct collapse black hole scenario) accreting below the Eddington rate, or from light seeds (e.g. remnants from the first generation of stars) experiencing phases of super-Eddington accretion during galaxy merging events ([11–17, 41–44]). The bottom panels of Figure 3 show the comparison of JADES GN 1146115 with the CAT semi-analytical models from [11, 12], who envisage both scenarios, in a snapshot at $z=7$. The Eddington-limited, heavy-seeds scenario (grey small scattered symbols) fails to reproduce the properties of JADES GN 1146115. Indeed, in order to reproduce the large black hole masses observed at high redshift without exceeding the Eddington limit, this scenario requires black holes to be accreting close to the Eddington limit for most of the time. Therefore, the high mass black holes, predicted by this scenario, are not found at the significantly sub-Eddington rates as observed in our object. Additionally, this scenario can reproduce a very overmassive nature of black holes ($M_{\text{BH}}/M_{\text{star}} \sim 0.1$) only for low mass galaxies ($M_{\text{star}} \sim 10^6 - 10^7 M_\odot$), or more moderately overmassive black holes ($M_{\text{BH}}/M_{\text{star}} \sim 0.01$) in more massive galaxies, hence is not capable of reproducing the $M_{\text{BH}}/M_{\text{star}} = 0.43$ observed in JADES GN 1146115 with $M_{\text{star}} = 2 \times 10^9 M_\odot$. On the contrary, the models show that, even starting from light seeds, allowing super-Eddington accretion bursts (red shaded contours) can reproduce properly the observed properties of our object. It may sound counter-intuitive that super-Eddington scenarios can reproduce better the relatively quiescent AGN in JADES GN 1146115. The fact is that super-Eddington accretion phases allow the black hole to grow rapidly in those short (1-4 Myr) bursts, while the resulting strong feedback makes the black hole

lack gas to accrete significantly for long periods. Essentially, the short super-Eddington bursts make the black hole reach high masses while allowing it to be dormant for long periods, hence making it more probable to be observed in such a dormant phase.

We note that the same result is found also when comparing with other cosmological simulations. In the Methods we show the comparison with the FABLE simulations [45]: heavy seeds with Eddington-limited accretion fail to reproduce the properties of our source, while light seeds experiencing super-Eddington accretion can match its observed properties.

It is tempting to speculate that our result favors light seed models. However, the same result would also hold if the models had started with heavy seeds. The key feature that allows the properties of JADES GN 1146115 to be matched is the fact that accretion goes through super-Eddington phases, regardless of whether the seeding is heavy or light.

However, we note that most of the simulated overmassive, low accretion rate BHs reside in hosts with SFRs an order of magnitude higher than that of JADES GN 1146115 (meaning that their star formation is outpacing the black hole growth, moving them towards the local scaling relation). The discrepancy between simulations and observations in terms of SFR may indicate that the feedback implementation in the models probably needs to be revisited.

Within the same context, it is interesting to note that for the BH accretion rate and SFR inferred for JADES GN 1146115, at the time of the observation the system is moving parallel to the local $M_{\text{BH}} - M_{\text{star}}$ relation, with no indication that it will be approaching it in the near future. In order to become consistent with the local relation, the galaxy should start a new phase in which it forms stars at a much higher rate, possibly via significant gas inflow, without allowing the black hole to accrete significantly. It is not obvious how this can happen [46]. As mentioned, the SFH indicates that the galaxy has been forming stars at the same rate for a few 100 Myr. A possibility is that at later epochs the gas accretes onto the galaxy with larger angular momentum [47, 48], which becomes fuel for star formation in the disc, while it can hardly reach the black hole (consistent with the inside-out growth scenario [49, 50]). Possible support for this comes from the fact that the metallicity of the gas in the host galaxy, as inferred from the detection of the [O III] λ 4363 auroral line (see Methods), places JADES GN 1146115 well below the mass-metallicity relation at the same epoch, as illustrated in Figure 10. This indicates that the galaxy has likely accreted very low metallicity gas from the intergalactic medium (IGM). The comparison of dynamical mass with stellar mass does indeed suggest a large gas fraction in the host galaxy (although with large uncertainty, $f_{\text{gas}} = 0.74^{+0.13}_{-0.21}$, see Methods), not unusual at such high redshifts. Yet, the inferred long depletion time ($\tau_{\text{dep}} \sim 1.6$ Gyr), longer than for normal star forming galaxies, indicates that star formation is inhibited, possibly by the heating and turbulence induced by the AGN.

Finally, we argue that dormant, overmassive black holes in galaxies with low SFR, such as JADES GN 1146115, are probably quite common in the early Universe. Indeed, finding one of them out of 35 spectroscopically targeted galaxies at $z > 6$ in the GOODS-N field, in a single tier of the JADES survey, is remarkable, as the JADES selection function at $z > 6$ primarily favours Ly α drop-outs, i.e. galaxies with blue colors, which

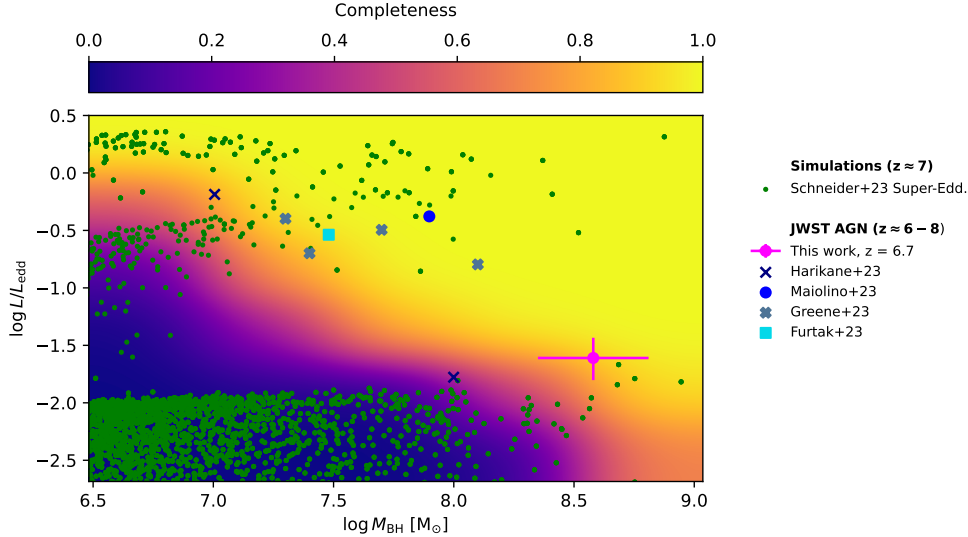


Fig. 4 Completeness simulation results on the Eddington ratio versus black hole mass plane. Points colored in blue hues show the previously discovered JWST sources at $6 < z < 8$, as in Figure 3. The dark green points show the simulated AGN (at $z \sim 7$) in the scenario of super-Eddington bursts. JADES GN 1146115 is indicated with magenta circle and errorbars. The color shading indicates the completeness of the JADES spectroscopic survey in detecting black holes with a given mass and accreting at a given rate relative to Eddington. It can be readily seen that most of the low accretion rate AGN predicted by super-Eddington bursts lie in the sub-50% completeness region and that JADES GN 1146115 overlaps them at the edge of the high completeness region.

disfavours the selection of high- z with low star formation rates [51]. Additionally, the very low BH accretion rate makes the intensity of the broad lines very weak and much more difficult to detect relative to all other AGN found at high- z . The fact that, out of the three Type 1 AGN at $z > 6$ currently found by JADES, one is a dormant black hole in a relatively quiescent galaxy, despite all the selection effects against this class of objects, indicates that they must be much more numerous and much more common than active AGN in star forming galaxies. We have performed a completeness simulation to infer the capability of the JADES survey in detecting black holes with a given mass and accretion rate, at the same redshift as JADES GN 1146115 (see Methods for details). The results are shown in Figure 4, where light background colors indicate higher levels of completeness. As expected, at a given black hole mass, more black holes accreting more vigorously are easier to detect. The comparison with the simulations for light seeds accreting with super-Eddington bursts at $z \sim 7$ (green points, from [11, 12]) reveals that JADES GN 1146115 overlaps with the high-mass tail of dormant black holes in the region where a few of these become detectable in the JADES survey. However, this is just the tip of the iceberg, as the majority of these dormant black holes are expected to be undetected. Specifically, none of the simulated BHs from [11, 12] with masses lower than $10^8 M_{\odot}$ and Eddington ratios below 0.03 are detectable in the JADES survey. This fraction becomes $\sim 44\%$ in the higher BH mass range tail

probed by JADES GN 1146115 ($10^8 < M_{\text{BH}} < 10^9 M_{\odot}$). The plot also confirms that the several black holes found by JWST accreting close to the Eddington rate (blue symbols) are preferentially selected in this phase only because they are much more luminous and easier to detect. Some of the AGN observed at high redshift are seen accreting at super-Eddington [2, 21] rates, confirming the existence of (short) super-Eddington phases. JADES GN 1146115 is detected, despite being dormant, because it is just above the detectability threshold; yet, our result suggests that the majority of black holes at high redshift are dormant and apparently rare only because they are much more difficult to detect.

1 Methods

1.1 Data description and reduction

All data used herein has been obtained from the JADES survey, the full description of which is available in [52]. Here we make use of data from the Medium/HST in GOODS-N tier, which consists of a single Near Infrared Spectrograph (NIRSpec) spectrum in prism and R1000 gratings. We also make use of the accompanying Near Infrared Camera (NIRCam) wide-band imaging data.

1.1.1 NIRSpec

The full description of the NIRSpec data used is available at [2]. A brief summary is provided here for completeness. The observations in the Medium/HST tier in GOODS-N consisted of three medium resolution gratings (G140M/F070LP, G235M/F170LP, G395/F290LP) and low resolution prism. The exposure time was 1.7 hours per source in prism and 0.8 hours per source in the medium gratings. The data was processed according to procedures laid out in [53] and other similar JADES papers, such as [54]. A full description of the data reduction procedure will be presented in Carniani et al. in prep, here we note that the spectral data was reduced using the pipeline developed by NIRSpec GTO team and the ESA NIRSpec Science Operations Team. As the primary interest of this study was the properties of the central, unresolved region, containing the AGN, we use the 1D spectra extracted from the central 3 pixels, corresponding to $0.3''$, of each 2D spectra. Path-loss corrections were calculated for each observation, taking into account the intra-shutter position, assuming a point-source geometry and a 5-pixels extraction box. Due the compact nature of the object, to maximise the S/N, we use 3 pixel extractions; even though a 3-pixel box is not the extraction box we optimised the path-loss corrections for, we compared directly the two spectra and found no systematic difference within the uncertainties.

The full obtained prism spectrum is shown in Figure 5.

1.1.2 NIRCam

The imaging data consisted of 7 wide (F090W, F115W, F150W, F200W, F277W, F356W and F444W) and 1 medium (F410M) filter bands of the NIRCam instrument in the GOODS-N field. We also use imaging in the F182M and F210M medium bands. The photometric data reduction procedure is presented in [55, 56] and [50] with a

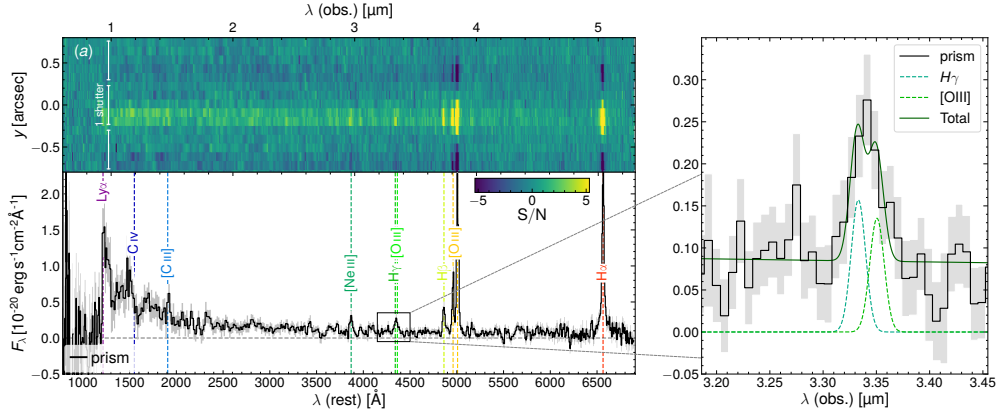


Fig. 5 Full prism spectrum of JADES GN 1146115. The top panel shows the 2D spectrum with the y axis representing the shutter pitch and yellow portions showing more positive flux. The bottom panel shows the extracted 1D spectrum with the Lyman break and emission line locations indicated by colored vertical lines. The panel to the right shows a zoomed-in view on the blended H γ and [O III] λ 4363 feature along with its decomposition into two Gaussian profiles.

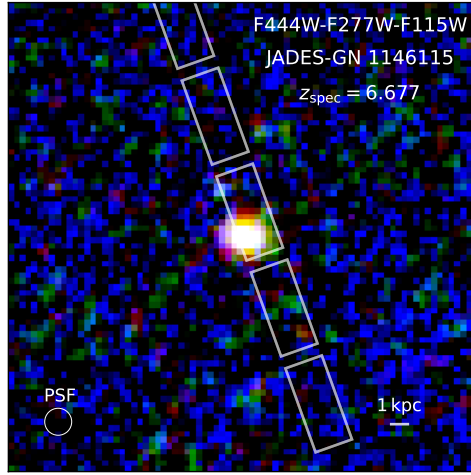


Fig. 6 A red-green-blue (RGB) image of the AGN and galaxy in the F444W, F277W and F115W bands. A 1 kpc physical scale bar is overlotted alongside the FWHM of the PSF in the F444W band. The position of the NIRSpec slit is also overlotted.

full description to be made available in Tacchella et al. in prep. In summary, we use v1.9.2 of the JWST calibration pipeline [57] together with the CRDS pipeline mapping context 1039. Stages 1 and 2 of the pipeline were run with our own sky-flat provided for the flat-fielding, otherwise keeping to the default parameters. After Stage 2, custom procedures were performed to account for $1/f$ noise and subtract scattered light artifacts, "wisps", along with the large scale background. Astrometric alignment was performed using a custom version of JWST TweakReg, with corrections

derived from HST F814W and F160W mosaics along with GAIA Early Data Release 3 astrometry. The images of individual exposures were then stacked in Stage 3 of the pipeline with the final pixel scale being 0.03" per pixel.

1.2 Spectral fitting and further spectral analysis

In order to identify the broad component in the $H\alpha$ line, we use a Bayesian method to model it with two components models - one containing only narrow emission in the $H\alpha$ line, $[\text{N II}]\lambda\lambda 6548, 6583$ and $[\text{S II}]\lambda\lambda 6716, 6731$ doublets, the broad-line model included a broad component in the $H\alpha$ line. Narrow-line widths were constrained to be the same for every line, the ratio of the $[\text{N II}]$ doublet fluxes was fixed to 3 (as from their Einstein coefficients ratios), the $[\text{S II}]$ doublet fluxes remained independent but constrained to be within the flux ratio 6716/6731 range expected in the low and high density regimes (0.45 - 1.45, [58]). The priors on the peak widths were uniform with the fitted FWHM ranging between 700 and 1,500 km s^{-1} for the narrow, and between 1,500 and 11,500 km s^{-1} for the broad component, with the lower bound set by instrument resolution. The posterior is estimated with a Markov-Chain Monte-Carlo integrator, [59]. Redshifts for the narrow peaks and the BLR were fit independently with priors being set to narrow Gaussians centered on the overall redshift obtained through visual inspection and widths inferred from the pixel scale in redshift space. Line peak heights utilized log-uniform priors.

Performance of the two models was quantified using the Bayesian information criterion (BIC), defined as

$$BIC = \chi^2 + k \ln n, \quad (1)$$

where k is the number of free parameters and n , the number of data points fitted. Following the criteria in [2], we require $\Delta BIC = BIC_{\text{Narrow}} - BIC_{\text{Narrow+Broad}}$ to be above 5 for a robust detection. In addition, we require the fitted broad component to have a significance of at least 5σ . The significance of the broad component of JADES GN 1146115 was found to be 9σ and ΔBIC came out to be 31. The full summary of the fit is shown in a corner plot in Figure 7. As can be seen there, the data is quite constraining on the different components with no significant degeneracies between them.

We note that the spectrum shown in Figure 1 appears to have a feature at $\lambda \approx 4.94 \mu\text{m}$, the origin of which is currently unclear. In the 2D spectrum, this feature is offset by 1-2 pixels, suggesting that it might be $H\alpha$ line of a foreground galaxy at $z \approx 6.53$. However, one of the four exposures has an outlier at this location Figure 8; although this has been masked, the feature might be a residual artefact. For these reasons, we choose to mask this feature in the final fit, although its inclusion would not significantly affect the results.

To check for evidence of outflows, we fit the $H\beta$ line together with the $[\text{O III}]$ doublet in the medium resolution data. For this purpose we fit these lines first with single components constrained to have the same width, with the ratio of $[\text{O III}]$ doublet peaks fixed at 3, then introduce a broader outflow component into each line, and finally we fit a broad component to $H\beta$. We find that single narrow component fits are preferred for each line, showing no evidence for outflows or a broad component in $H\beta$, as can be seen in Figure 9. The measured FWHM of the narrow lines in R1000 was

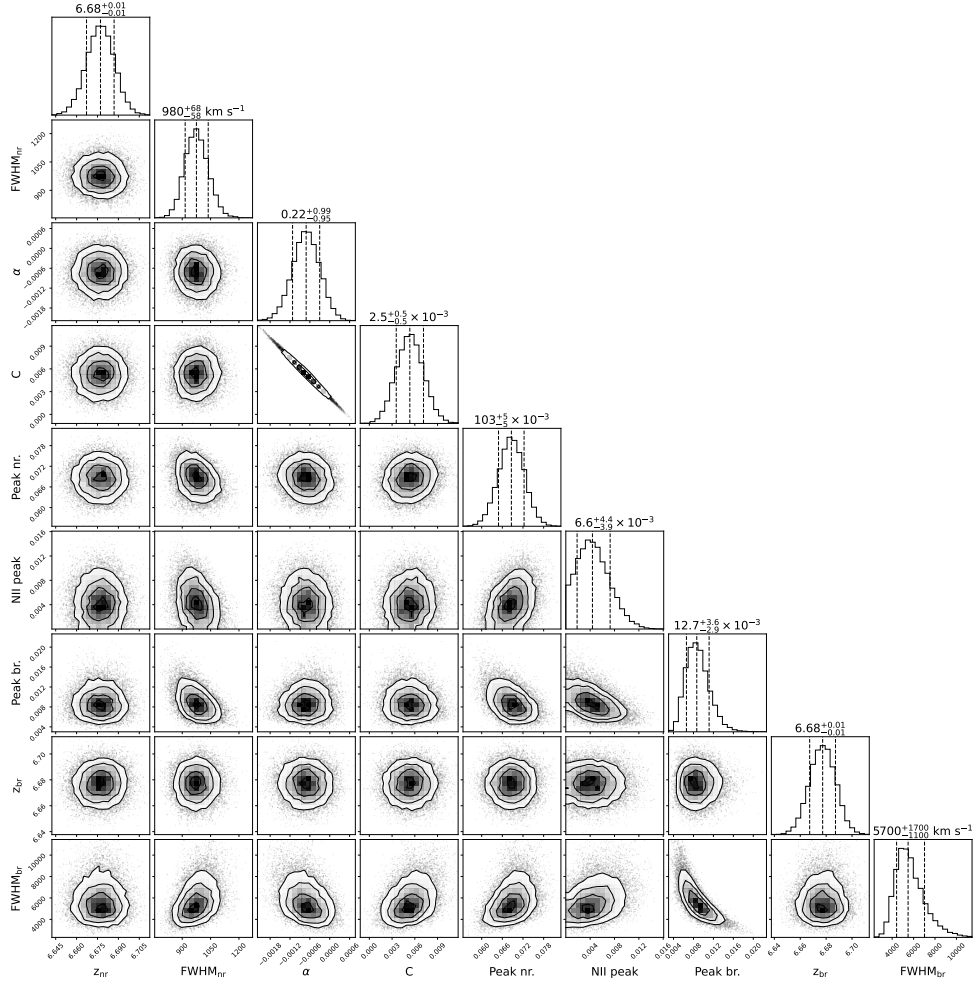


Fig. 7 A corner plot summarizing the MCMC fit results of the H α profile. Here α and C are the continuum slope and normalization respectively, "Peak nr." and "Peak br." show the peak heights of the narrow and broad H α components respectively. The FWHM values given are not corrected for instrumental broadening. The total spectrum was normalized to unity before fitting, hence peak heights are unitless here. The [S II] doublet parameters are not shown as it is undetected.

225^{+11}_{-11} km s $^{-1}$, when corrected for instrumental broadening, which was 180 km s $^{-1}$ in the wavelength range considered.

We also utilize previous Hubble Space Telescope (HST) imaging of the source carried out in 2018 to check its variability and thus the presence of supernovae. Subtracting HST and JWST images taken in equivalent filters shows that the flux of the source varied by no more than 5% over the 4 year period in the observed frame, corresponding to <5% variability over a 6 month period in the object's frame. This

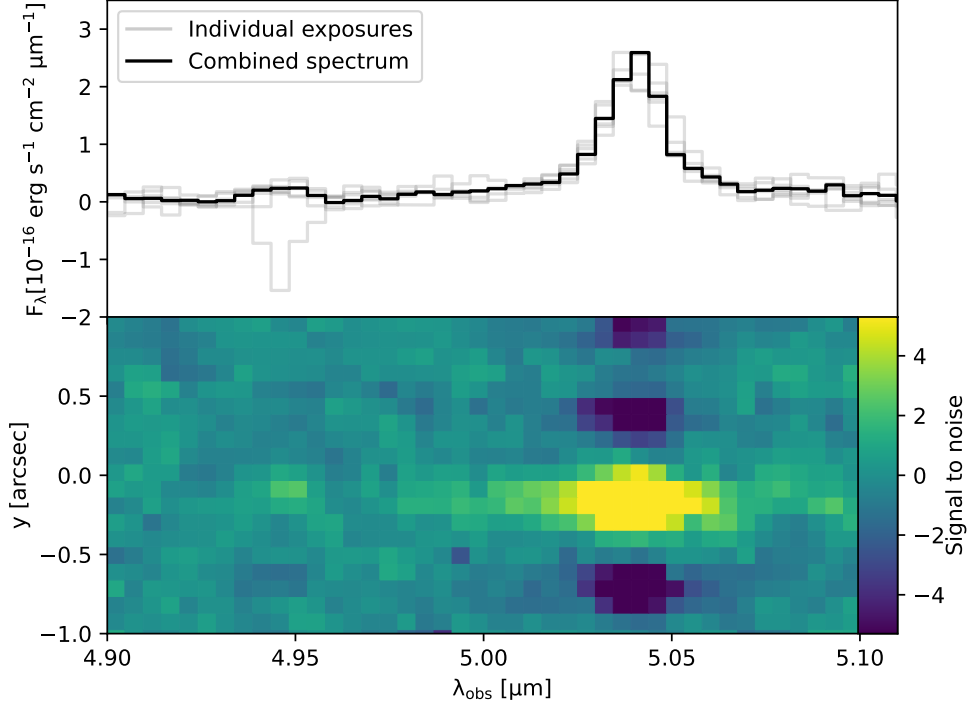


Fig. 8 Combined spectrum around $H\alpha$ compared with the individual exposures. Grey lines in the top panel show the individual exposures, with the stacked spectrum shown in black. The bottom panel shows the 2D spectrum zoomed in on the same region. It can be seen that there is an outlier in the location of the artefact at $\lambda \approx 4.94 \mu\text{m}$. The 2D cutout also shows the slight spatial offset of the feature.

conclusively shows that our observed broad component can not be the product of a recent supernova explosion in the galaxy.

In addition, we leverage the higher depth of the prism to fit weaker emission lines, in particular $H\gamma$, $[\text{O III}]\lambda 4363$, $[\text{Ne III}]\lambda 3869$ and $[\text{O II}]\lambda 3727$, as the $[\text{O III}]$ auroral line may be used to constrain metallicity while the remaining lines are candidate diagnostics for Type 2 AGN. Each line has been fit with a single Gaussian profile together with $H\beta$ and the $[\text{O III}]$ doublet with redshift and FWHM fixed by the latter. We note that, although the $[\text{O II}]\lambda 3727$ line is part of a doublet, said doublet is completely blended in the prism spectrum and the overall detection significance ends up being marginal (Table 1). All narrow emission lines fitted are summarized in Table 1. It should be noted that we carry out our fitting using spectra extracted from the central 3 pixels of the source in order to enhance the S/N of lines as the region of emission is compact due to the AGN nature of the source. However, the flux corrections applied by the reduction pipeline are geared towards the 5 pixel extracted spectra, we thus redo our fits using the 5 pixel spectra and find that the derived line fluxes differ by less than 1σ .

Our tentative (3.6σ) detection of [O III] λ 4363, together with the [O III] $\lambda\lambda$ 5007,4959 doublet can be used to estimate electron temperature based on their ratio. The electron density can not be reliably estimated from the spectrum due to lack of an [S II] $\lambda\lambda$ 6716,6731 detection, however we note that the inferred electron temperature is relatively insensitive to density between 100 and 10,000 cm^{-3} , typical of narrow line regions of AGN [60]. We thus assume electron density of order of 1000 cm^{-3} and calculate the electron temperature to be $T_e \approx 25000_{-4800}^{+3200}$ K. Assuming the main ionization mechanism to be AGN activity we follow the methods from [61] to derive the contributions to metallicity from different ionic species of oxygen - $12 + \log(O^{++}/H) = 7.28_{-0.1}^{+0.16}$ and $12 + \log(O^+/H) < 6.13$, the latter value presenting an upper limit due to the low detection significance of [O II] λ 3727. The contribution of higher ionization oxygen species is likely negligible due to lack of [O IV] and He II line detections. He II lines have similar ionization potential to [O IV] but helium is much more abundant, thus their lack of detection implies that the radiation is not sufficiently hard to produce significant amounts of highly ionized oxygen. The final oxygen abundance ratio estimate is thus $12 + \log(O/H) = 7.32_{-0.10}^{+0.16}$, corresponding to $Z \approx 0.04Z_\odot$. However, the [O III] λ 4363 line is heavily blended with H γ in prism, therefore the simple two-Gaussian fit may underestimate the relevant uncertainties. As a conservative estimate we obtain a lower limit on the [O III] λ 4363 flux by fitting the blended lines with a single Gaussian profile and subtracting from its flux the H γ flux obtained in a fit without [O III] λ 4363 included. This method resulted in $F_{[\text{O III}]\lambda 4363} \geq 9.1 \times 10^{-20} \text{ erg s}^{-1} \text{ cm}^{-2}$. Repeating the former analysis gives $T_e \geq 15000$ K and $12 + \log(O/H) \leq 7.72$. A lower limit on metallicity was derived by fitting the blended feature with [O III] λ 4363 only and results in $T_e \leq 34000$ K and $12 + \log(O/H) \geq 7.08$. These limits are consistent with the best-fit value and place our source somewhat below the mass-metallicity relation at similar redshifts (Figure 10). As a final check on these results we fit the blended [O III] λ 4363 and H γ feature by fixing the ratio of H β and H γ to the appropriate Balmer decrement and find $12 + \log(O/H) = 7.25_{-0.17}^{+0.20}$, which is completely consistent with the above estimates.

1.3 Estimation of the Black hole mass and accretion rate

As mentioned in the main text the broad component of H α can be used to infer the black hole mass by assuming the local scaling relations and, specifically, from the equation [18, 19]:

$$\log \frac{M_{\text{BH}}}{M_\odot} = 6.60 + 0.47 \log \left(\frac{L_{\text{H}\alpha}}{10^{42} \text{ ergs}^{-1}} \right) + 2.06 \log \left(\frac{\text{FWHM}_{\text{H}\alpha}}{1000 \text{ km s}^{-1}} \right) \quad (2)$$

The best fitting values for the broad component of H α (Full Width Half Maximum of 5700_{-1100}^{+1700} km s^{-1} and flux of $27.3_{-4.0}^{+4.1} \times 10^{-19}$ $\text{erg s}^{-1} \text{ cm}^{-2}$) give $\log M_{\text{BH}}/M_\odot = 8.23_{-0.20}^{+0.24} \pm 0.33$, with the latter uncertainty coming from systematic scatter on Equation 2. Coupled with the bolometric luminosity of 3×10^{43} erg s^{-1} , estimated from the broad component of H α (following the scaling relation given by [20]), gives an Eddington ratio $\lambda_{\text{Edd}} = 0.009_{-0.003}^{+0.005}$, with a systematic scatter of 0.5 dex.

It is difficult to estimate dust attenuation in this object. The lack of broad H β does not provide strong constraints: even assuming a standard case-B recombination ratio

Line	Flux ($\times 10^{-19}$ erg s $^{-1}$ cm $^{-2}$)	S/N	Disperser
[S II] λ 6731	< 1.5	1.38 σ	prism
[N II] λ 6585	2.84 $^{+1.06}_{-1.13}$	2.0 σ	prism
H α	36.2 $^{+2.3}_{-2.2}$	25 σ	prism
[O III] λ 5007	46.7 $^{+1.3}_{-1.4}$	159 σ	R1000
[O III] λ 4959	15.4 $^{+0.43}_{-0.46}$	65 σ	R1000
H β	6.66 $^{+0.81}_{-0.82}$	29 σ	R1000
[O III] λ 4363	2.39 $^{+0.65}_{-0.65}$	3.60 σ	prism
H γ	2.77 $^{+0.68}_{-0.70}$	3.96 σ	prism
[Ne III] λ 3869	3.87 $^{+0.94}_{-0.91}$	3.63 σ	prism
[O II] λ 3727	1.78 $^{+0.66}_{-0.67}$	2.64 σ	prism

Table 1 Summary of all narrow lines measured in JADES GN 1146115. Column one contains the names of each line, the second column - measured flux along with uncertainties, the final two columns contain signal to noise ratios and disperser in which each line was measured. For lines with S/N < 3 σ the measured fluxes were treated as upper limits, for < 2 σ detections, the 2 σ upper limit is quoted instead.

of 2.8, the broad H α line flux implies that the broad H β is not detectable. We therefore assume, as found for other AGN at high-z, that the bulk of the obscuration towards the Broad Line Region also affects the narrow components [64]. From the observed ratio of the narrow components of H α and H β ($5.51^{+0.86}_{-0.69}$), and assuming an SMC extinction law (appropriate for high-z AGN, [65, 66]), we infer $A_V = 2.00^{+0.44}_{-0.41}$ mag. The extinction corrected black hole mass, bolometric luminosity and Eddington ratio are $\log M_{\text{BH}}/M_{\odot} = 8.61^{+0.24}_{-0.27} \pm 0.33$, $L_{\text{bol}} = 2 \times 10^{44}$ erg s $^{-1}$, and $\lambda_{\text{Edd}} = 0.024^{+0.011}_{-0.008}$, respectively, with the same systematic scatter of 0.5 dex. The extinction correction is uncertain due to the use of the narrow lines, however, the extinction-corrected values are still consistent with the uncorrected ones within 2 σ , hence our conclusions are not significantly altered by the presence of dust. Additionally, in the next section we show that fitting the nuclear source detected by NIRCcam with a dust-reddened AGN slope results into an extinction consistent with that inferred from the narrow lines. In the next section we also infer the Bolometric luminosity from the fitting of the nuclear SED and, although with large uncertainties, independently obtain a value consistent with that obtained from the broad component of H α .

We note that even without correcting for extinction, the resulting *lower limit* on the black hole mass would still imply a BH-to-stellar mass ratio several 100 times above the local relation.

1.4 Morphological/photometric fitting and stellar population properties

To constrain the stellar mass and star formation rate of the host galaxy we employ fractional spectral energy distribution (SED) fitting. To do this we employ the tool **ForcePho** (Johnson+, in prep), which enables us to forward model the light distribution using a combination of Sérsic profiles. We perform spatially resolved photometry with **ForcePho** following the methodology detailed in [50, 56]. In short we model the

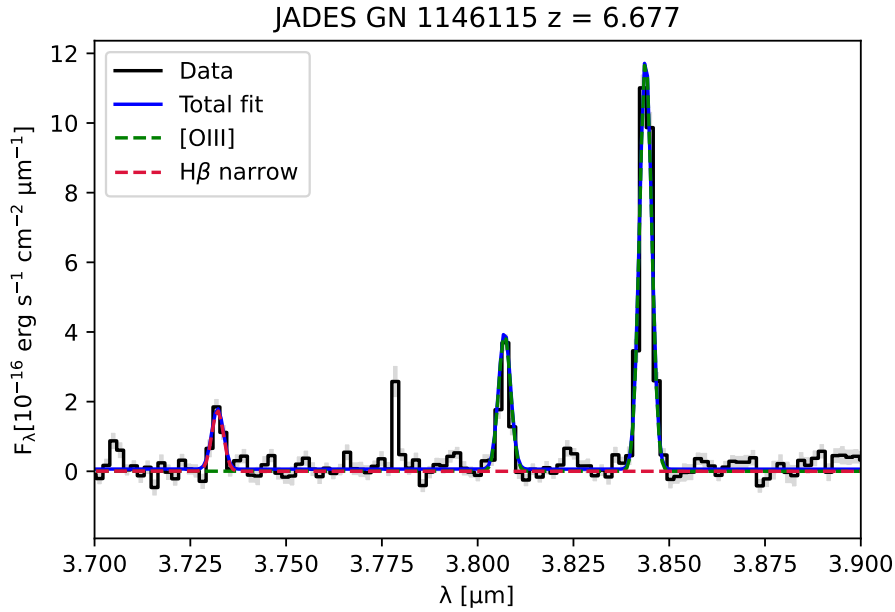


Fig. 9 Grating spectrum zoomed around H β and [OIII] along with the best fit model. It can be seen that the data is well explained by single component fits to each line, indicating no significant outflows.

AGN and host galaxy as a central point source component and underlying host galaxy component respectively and fit the light distribution in the individual exposures of all 10 NIRCcam bands simultaneously. This enables us to obtain accurate spatially resolved fluxes and morphological parameters for the galaxy. This approach has been used previously in [2, 50, 56].

Fig. 11 shows the data, residual, model, and point-source subtracted host galaxy for the ForcePho fit. We can see that the galaxy + point-source model has fit the data well without leaving significant residuals and the galaxy component appears bright enough for reliable photometry. The resulting, best-fit morphological parameters are reported in Table 2 and illustrates that the host galaxy is compact ($R_e \sim 140$ pc) with a disk-like profile (Sersic index $n \sim 1$).

The fluxes for the point-source component and host galaxy can be seen in Fig. 12. We see that the galaxy contains significantly more flux in the blue bands, whilst the contribution from the point-source AGN component increases in the red bands.

The next stage is to fit this spectral energy distribution in order to obtain the stellar population properties of the host galaxy. To do this we use the Bayesian SED fitting code **Prospector** [67], which uses Flexible Stellar Population Synthesis [FSPS 68] with MIST isochrones [69], nebular line and continuum emission [70] and a Chabrier [71] initial mass function (IMF). We also use the Bayesian SED fitting code **BAGPIPES** [22], which uses stellar population models of Bruzual & Charlot [72], alongside nebular line and continuum emission [70] with a Kroupa [73] IMF. For both codes, we include a

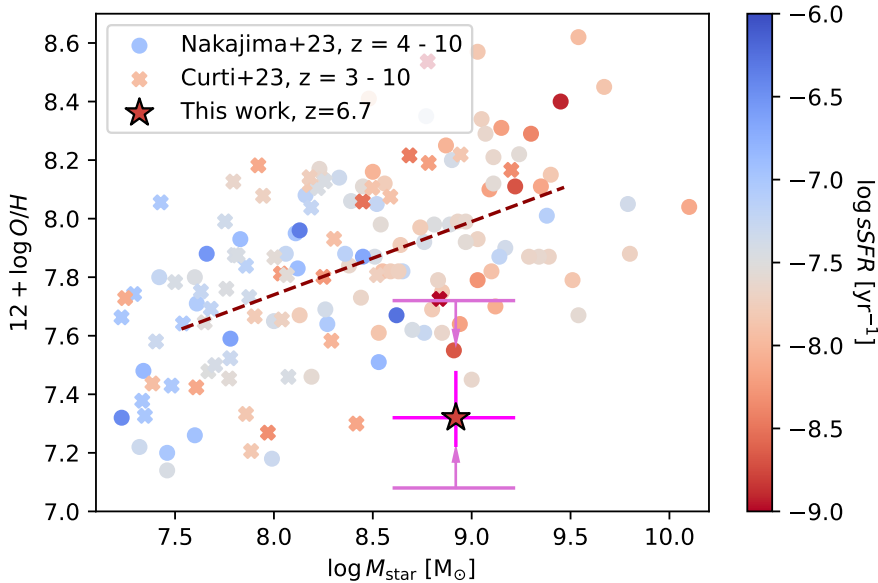


Fig. 10 Location of JADES GN 1146115 (large star with magenta errorbars) relative to the mass-metallicity relation at $z = 4 - 10$ obtained by [62] and [63] (circles and crosses) whose best fit is shown with the brown dashed line. The lighter colored magenta bars show the upper and lower limits for the metallicity of JADES GN 1146115. All markers are colored according to their specific star formation rate, $\log(sSFR)$.

flexible two component dust model following [74] consisting of a birth cloud component (affecting only light from the the birth clouds themselves, e.g. stars younger than 10 Myr) and a separate ‘diffuse’ component (affecting light from all sources). We assume a flexible star-formation history (SFH) with a continuity prior [75], where we fit for the ratio between the six SFH bins. Finally, we exclude the F410M and F356W filters from the fit as those contain the [O III] $\lambda\lambda 5007, 4959$ doublet and thus may have been contaminated by AGN ionization. This can be seen in the SED in Fig. 12, where we see the host galaxy has increased flux in the F410M and F356W bands compared to the point-source despite these bands containing [O III] $\lambda 5007 \lambda 4959$. This suggests that emission line flux from the AGN may likely still be contributing the recovered host galaxy SED in these bands justifying our exclusion of these bands from the SED modelling.

Fig. 13 shows the resulting *Prospector* fit (black) to the observed photometry (yellow) with the χ values below. These fits yield a stellar mass of $\log(M_*/M_\odot) = 9.00^{+0.27}_{-0.25}$ and $\log(M_*/M_\odot) = 8.71^{+0.24}_{-0.52}$ and instantaneous star formation rates of $SFR = 1.48^{+0.95}_{-0.42} M_\odot/\text{yr}$ and $SFR = 1.25^{+1.13}_{-0.89} M_\odot/\text{yr}$ for *BAGPIPES* and *Prospector*, respectively. These results are consistent within 1σ thus we combine the chains given by each code for the final estimate - $\log(M_*/M_\odot) = 8.92^{+0.30}_{-0.31}$ and $SFR = 1.38^{+0.92}_{-0.45} M_\odot/\text{yr}$.

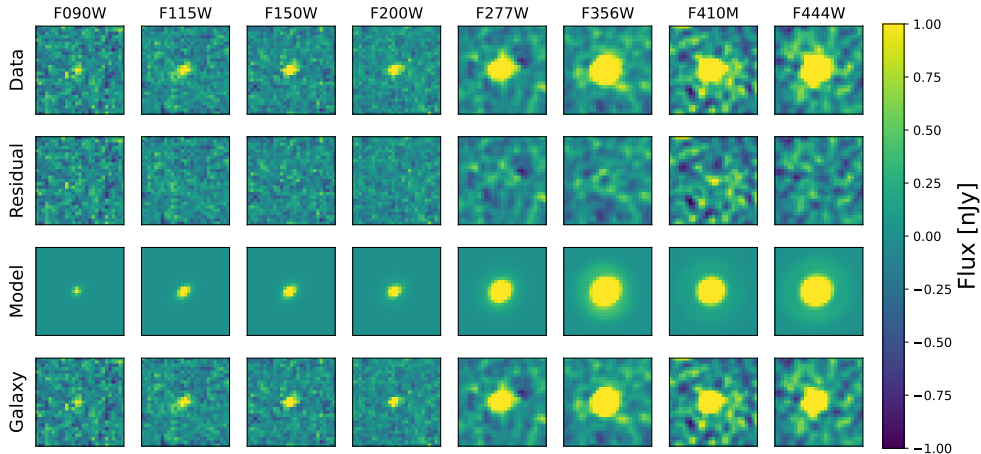


Fig. 11 The data, residual, model, and fluxes with the recovered galaxy component, for the point source and galaxy decomposition in the 8 JADES NIRCcam bands. The figure shows that the galaxy+point source model has fit the data well within all bands without leaving significant residuals.

We also test the effect of fitting the SED of the combined photometry, i.e. host galaxy + point-source, to estimate how much we would overestimate the stellar mass of the galaxy by not decomposing the AGN and host galaxy components. We find that the results are altered by less than 1σ .

All numeric properties of the host galaxy and its black hole obtained from the spectral and SED fitting are summarized in [Table 2](#).

[Fig. 14](#) shows the SFR of the host galaxy against lookback-time (and redshift) presenting the star-formation history as derived by both *Prospector* and *Bagpipes*. Both SFHs are consistent with a flat SFH although the two codes show systematic offsets, likely resulting from different assumptions in the codes, in particular the different stellar populations used.

We also fit the extracted point source (AGN) component with a reddened powerlaw with a fixed slope of $\beta = -1.55$ ($F_\lambda \propto \lambda^\beta$), corresponding to average slope of type 1, unobscured high-z quasars [76]. Assuming the SMC extinction curve, the resulting A_V is 2.68 ± 1.00 , which, while poorly constrained, is fully consistent with the value derived from spectroscopy. The bolometric luminosity inferred from the fitted λL_λ at $5,100\text{\AA}$, with the bolometric correction from [77], and corrected for absorption, is $4.6_{-3.2}^{+7.5} \times 10^{44} \text{erg s}^{-1}$, which is highly uncertain, but consistent with the value obtained from the broad component of $\text{H}\alpha$.

1.5 Black hole scaling relations with σ and dynamical mass

As discussed in [2], while high-z AGN are offset on the BH-stellar mass plane relative to the local relation, they are much closer to the local relation between black hole mass and stellar velocity dispersion σ_* relation and to the local relation between black

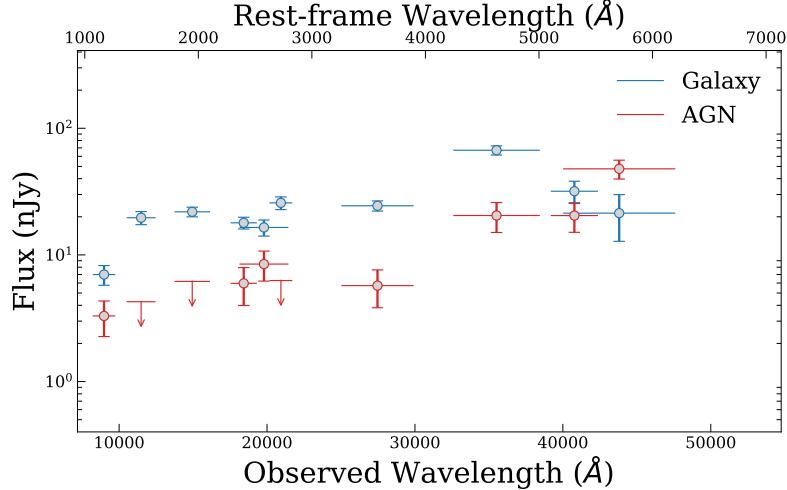


Fig. 12 The spectral energy distribution for the point source and galaxy decomposition in the 10 NIRCcam bands. The figure shows that we have recovered a significant amount of the host galaxy’s flux within all bands and that the AGN SED is reddened.

hole mass and host galaxy dynamical mass. Here we explore the location of JADES GN 1146115 on the latter two scaling relations.

We use as a proxy of the velocity dispersion the width of the [OIII] line, $\text{FWHM} = 255 \pm 11 \text{ km s}^{-1}$, as measured from the medium resolution grating spectrum, deconvolved for the line spread function for compact sources. We then derive the stellar velocity dispersion by correcting gaseous velocity dispersion by 0.1 dex to obtain the stellar velocity dispersion, following [78], giving $\sigma_* = 121^{+6}_{-6} \text{ km s}^{-1}$. The resulting location of JADES GN 1146115 in Fig. 15, shown with a magenta circle, illustrates that our object is close to the local relation (solid line, with dispersion shown with a shaded region), as are other high- z AGN previously measured by JWST.

We also utilize the host galaxy parameters to estimate its dynamical mass using the same approach as in [2, 4], which makes use of the equation:

$$M_{\text{dyn}} = K(n)K(q) \frac{\sigma_*^2 R_e}{G}, \quad (3)$$

where $K(n) = 8.87 - 0.831n + 0.0241n^2$, with Sérsic index n , $K(q) = [0.87 + 0.38e^{-3.71(1-q)}]^2$, with q being the axis ratio [79], R_e - the estimated effective radius and σ_* - the stellar velocity dispersion. Utilizing Equation 3 along with values for R_e , n and q given by ForcePho (summarized in Table 2) gives $\log M_{\text{dyn}}/M_\odot = 9.50^{+0.04}_{-0.04}$. We caution that the errors on this estimate are likely underestimated due to the absence of high resolution spectral observations for JADES GN 1146115. The position of our object with respect to other JWST sources and the local scaling relation on the $M_{\text{BH}} - M_{\text{dyn}}$ and $M_{\text{BH}} - \log \sigma_*$ star plane is shown in Figure 15. The source remains above the local relation, however, the difference is not as severe as in the BH - stellar mass relation.

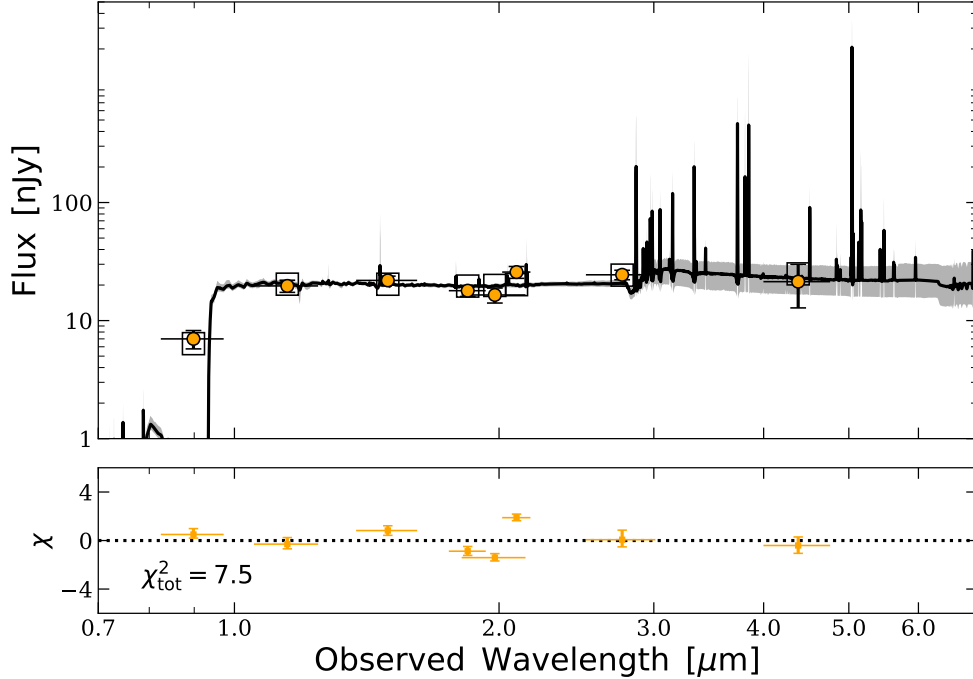


Fig. 13 Spectral Energy Distribution (SED) for the host galaxy fit by *Prospector*. Yellow points correspond to the observed photometry. Black squares correspond to the model photometry and the model spectrum is overplotted in black. The chi distribution of the observed to model photometry is shown below. We note that we do not fit the F356W and F410M bands due to strong contamination from the AGN. The figure shows that *Prospector* has fit the observed photometry well.

2 Gas fraction and star formation efficiency

Following our dynamical and stellar mass estimates we are able to obtain an estimate for the gas mass in the host galaxy, using $M_{\text{gas}} = M_{\text{dyn}} - M_{\text{star}}$, assuming little contribution from dark matter, especially at such early epochs, within the central few 100 pc. This gives $\log M_{\text{gas}}/M_{\odot} = 9.37^{+0.07}_{-0.14}$ and a gas fraction f_{gas} of $0.74^{+0.13}_{-0.21}$. The depletion time for our object can thus be estimated as $\frac{M_{\text{gas}}}{\text{SFR}} = 1.59^{+0.91}_{-0.85}$ Gyr. The depletion time given by the scaling relation from [80], assuming a star forming main sequence of the form given in [24], evaluates to 0.66 Gyr. While these values are consistent within the intrinsic scatter on the relation, as shown in Figure 16, this is still suggestive of star formation being inhibited relative to the population of normal star forming galaxies at this epoch.

3 Completeness analysis

In order to quantify the selection bias affecting the identification of AGN with broad emission lines, we run the fitting procedure described in 1.2 on simulated broad

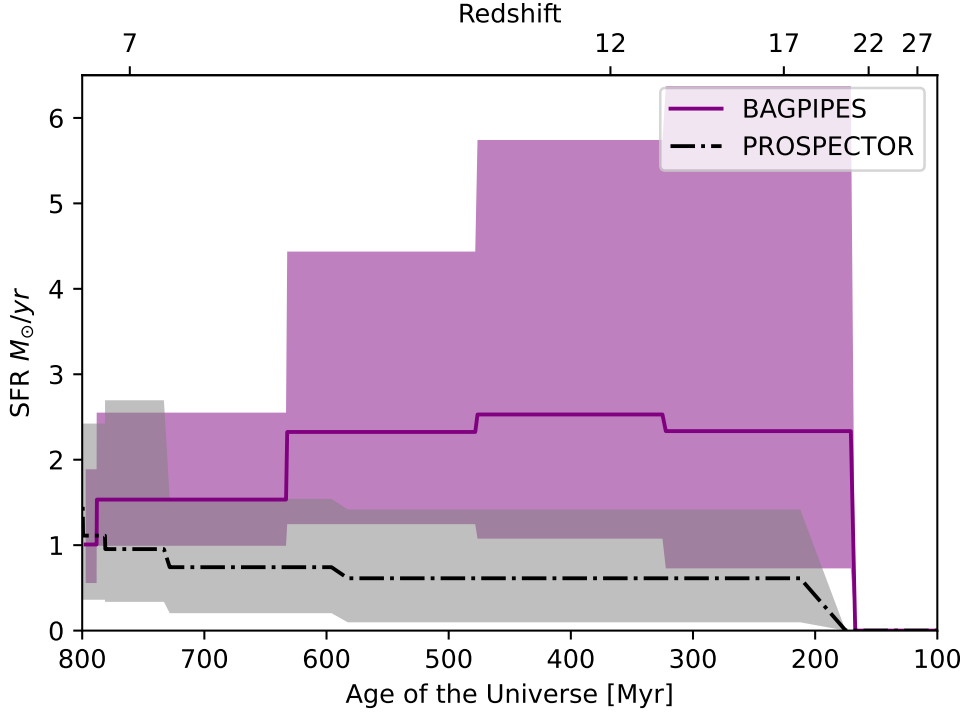


Fig. 14 A comparison between the SFHs given by the two different codes used. While both SFHs are quite uncertain, they consistently show that the galaxy experienced a roughly constant SFR between 1 and 2 $M_{\odot} \text{ yr}^{-1}$ for most of its lifetime.

$H\alpha$ profiles. These profiles were simulated by using the error extension of the prism data for JADES GN 1146115 to simulate Gaussian noise and adding Gaussian line profiles along with a power-law continuum on top of it. The FWHM and luminosity for the narrow $H\alpha$ component were uniformly sampled from $\text{FWHM} \in [200, 600] \text{ km s}^{-1}$ and $\log(L/\text{erg s}^{-1}) \in [42, 43]$ ranges respectively. Redshifts of the simulated sources were uniformly drawn from between 6 and 7. Continuum normalization was set to be 100 times smaller than the $H\alpha$ narrow peak height and slopes were sampled from a uniform distribution ($-1 < \alpha < 1$). The model grid for the broad component of $H\alpha$ was computed by varying $\log(L/\text{erg s}^{-1})$ between 41.75 and 43 in steps of 0.25 and the FWHM between 1000 and 10000 km s^{-1} in steps of 1000 km s^{-1} . In the lowest two FWHM bins we performed the simulation assuming the grating spectrum R1000 error extension to assuage the effects of prism's lower resolution. This yielded a 6x9 grid, each point of which contained 100 spectra simulated according to the above recipe.

The fitting of the simulated data was carried out with the same parameters as those described in 1.2. The completeness of each grid point was calculated as the ratio of the sources recovered according to our criteria (in terms of both broad line significance and ΔBIC) to the sources inserted. The final completeness function is presented in

Table 2 Properties of the host galaxy and its AGN obtained via imaging modelling, SED fitting and spectral analysis.

Quantity	Value
q	$0.51^{+0.04}_{-0.04}$
n	$0.94^{+0.07}_{-0.07}$
R_e [pc]	137^{+8}_{-8}
σ_* [km s $^{-1}$]	121^{+6}_{-6}
$\log(M_{\text{dyn}}/M_{\odot})$	$9.50^{+0.04}_{-0.04}$
SFR [M_{\odot}/yr]	$1.38^{+0.92}_{-0.45}$
$\log(M_*/M_{\odot})$	$8.92^{+0.30}_{-0.31}$
$\log M_{\text{BH}}/M_{\odot}$	$8.60^{+0.24}_{-0.22}$
λ_{EDD}	$0.024^{+0.011}_{-0.008}$
$12 + \log(O/H)$	$7.32^{+0.16}_{-0.10}$
T_e [K]	25442^{+3215}_{-4810}
A_V	$2.00^{+0.44}_{-0.41}$

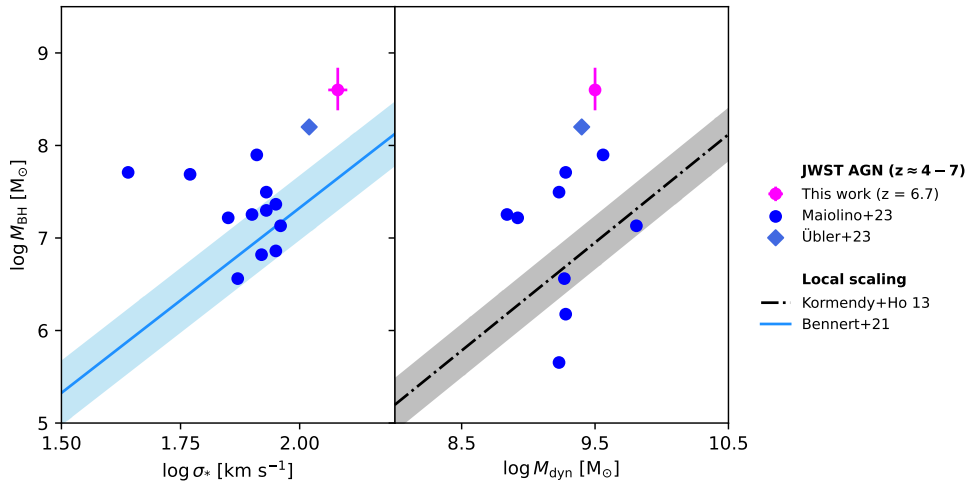


Fig. 15 Location of JADES GN 1146115 (magenta point) on the black hole mass versus stellar velocity dispersion (left) and versus dynamical mass of the host galaxy (right). Other high- z AGN found by JWST are shown with blue symbols. The black dash dotted line shows the local $M_{\text{BH}} - M_{\text{bulge}}$ relation from [40]. The solid blue line shows the $M_{\text{BH}} - \sigma_*$ relation from [39]. Shaded areas show the scatter around these relations, while not yet on the local relations, the offset of JADES GN 1146115 is much less severe than in the BH-stellar mass diagram.

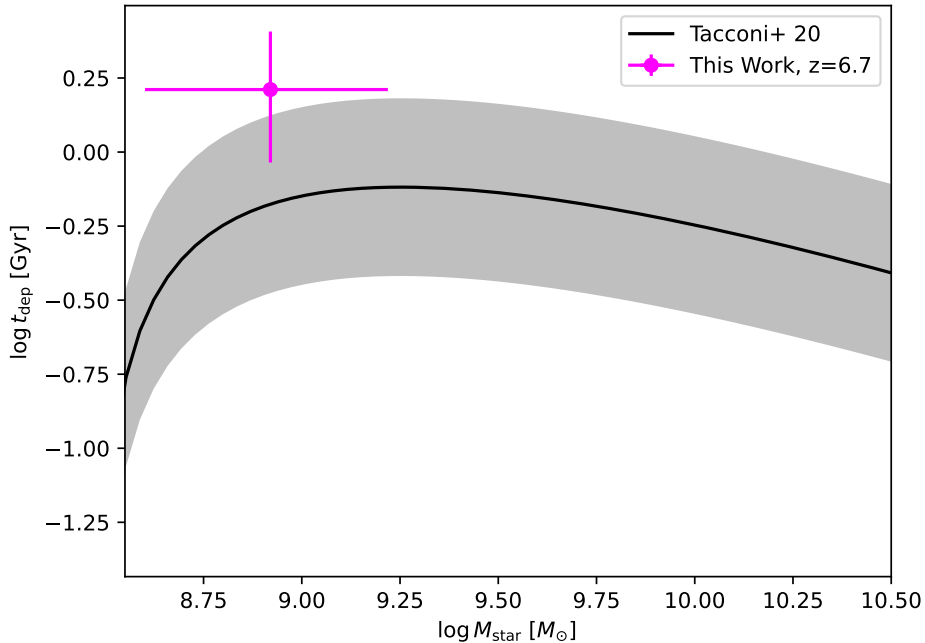


Fig. 16 Location of JADES GN 1146115 (magenta point) with respect to the depletion time versus stellar mass scaling relation for sources with the same SFR taken from [80] (solid black line). The grey shading represents the ~ 0.3 dex intrinsic scatter on the relation.

Figure 4 and shows that we are inherently biased against highly sub-Eddington black holes predicted by simulations, as most of those lie in regions of low completeness. We caution that the procedure described here only provides completeness with respect to the final step of AGN selection - the fitting of the BLR - and only covers the medium-depth tier of the JADES survey. The full selection function for the JADES survey is more complex as it spans multiple survey tiers, telescope instruments and source selection methods. Its full treatment is thus beyond the scope of the paper and our results here should be regarded as closer to an upper limit.

4 Comparison with the FABLE simulations

In order to put our work in greater context we also compare the properties of our source to predictions from the FABLE (*Feedback Acting on Baryons in Large-scale Environments*) [45] simulations. These are carried out with the massively parallel AREPO code [81] with new comoving $100 h^{-1}$ Mpc boxes. We consider both Eddington-limited and super-Eddington accretion, bounding our black hole Bondi-Hoyle-Lyttleton accretion rate in two different simulations by 1 and $10\times$ Eddington. Details regarding other

subgrid models, which are largely based on the Illustris galaxy formation models [82], can be found in [45].

A comparison between the simulated sources from FABLE and our object is provided in Figure 17, with the same coding as in Fig.3, i.e. gray symbols show the Eddington-limited scenarios and the red contours the distribution of simulations in which super-Eddington accretion is allowed. As can be seen there, the super-Eddington simulation is able to produce more massive black holes with respect to both luminosity and stellar mass in comparison to the Eddington-limited simulation, resulting in a better match with our observations. However, JADES GN 1146115 still lies above our super-Eddington simulations in the right-hand $M_{\text{BH}} - M_{\text{star}}$ plot, likely due to the FABLE simulations lacking in volume. To better sample a larger volume we also include simulation data from zoom simulations of a massive protocluster ($M_{\text{h}} > 10^{12} M_{\odot}$ at $z=6.66$), previously used in [15], that is taken from the larger Millennium simulation volume of $500 h^{-1} \text{ Mpc}$ [83]. These points are shown to the right of both panels of Figure 17. The objects obtained in these simulations have stellar masses notably larger than inferred from JADES GN 1146115 and, in runs including super-Eddington accretion up to $10\times$ Eddington (and also earlier BH seeding and slightly weakened feedback, unlike the other FABLE results shown here, see [15]), have also more massive black holes. Although a more quantitative match will be explored with future tweaking of these simulations, these results qualitatively show that super-Eddington bursts more readily explain the properties and presence of objects like JADES GN 1146115, particularly in increasing the black hole to stellar mass ratio, relative to Eddington-limited scenarios.

We also note that, as with CAT sources discussed in the main text, most of the simulated highly sub-Eddington sources reside in the low completeness region of the JADES survey (Figure 18) and are thus hard to detect at these redshifts even with current instruments.

5 Acknowledgements

The authors would like to thank M. Volonteri and A. Fabian for helpful comments and useful advice. S.A. acknowledges support from Grant PID2021-127718NB-I00 funded by the Spanish Ministry of Science and Innovation/State Agency of Research (MICIN/AEI/ 10.13039/501100011033). W.B. acknowledges support by the Science and Technology Facilities Council (STFC), ERC Advanced Grant 695671 "QUENCH". AJB, AJC, JC, IEBW, AS and GCJ acknowledge funding from the "FirstGalaxies" Advanced Grant from the European Research Council (ERC) under the European Union's Horizon 2020 research and innovation programme (Grant agreement No. 789056). S.C acknowledges support by European Union's HE ERC Starting Grant No. 101040227 - WINGS. RM acknowledges support by the Science and Technology Facilities Council (STFC), by the ERC through Advanced Grant 695671 "QUENCH", and by the UKRI Frontier Research grant RISEandFALL. RM also acknowledges funding from a research professorship from the Royal Society. M.P. acknowledges support from the research project PID2021-127718NB-I00 of the Spanish Ministry of Science and Innovation/State Agency of Research (MICIN/AEI/ 10.13039/501100011033),

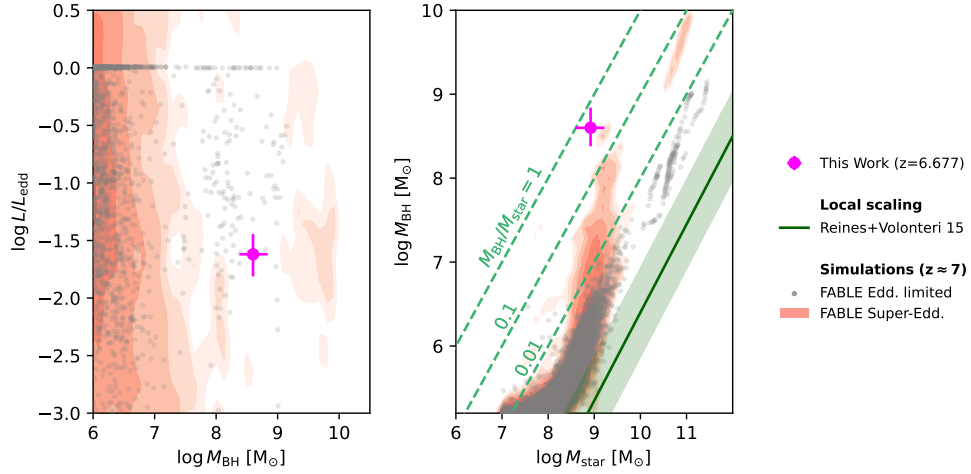


Fig. 17 A comparison between JADES GN 1146115 and sources in the FABLE simulation. The layout is the same as the bottom row of Figure 3, with sources from super Eddington simulations shown as red contours, while those from sub-Eddington ones are indicated by grey points. As in the case of the CAT models, the Eddington-limited heavy seed scenario fails to simultaneously explain the high BH-to-stellar mass ratio of JADES GN 1146115 and the very low accretion rate. Instead, the scenario in which BHs experience super-Eddington accretion phases can match the properties of JADES GN 1146115, although additional simulations would be needed to bridge the gap between small and large box simulations.

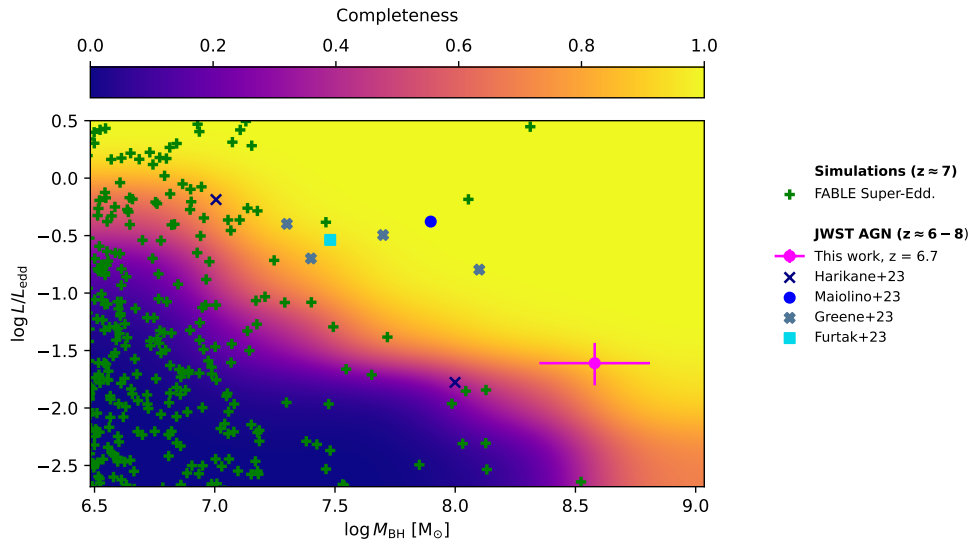


Fig. 18 Same as Figure 4 in the main text, except with super-Eddington models of the FABLE simulation, showing that dormant, post super-Eddington burst AGN are strongly biased against in the current surveys.

and the Programa Atracciòn de Talento de la Comunidad de Madrid via grant 2018-T2/TIC-11715. BER acknowledges support from the NIRCам Science Team contract to the University of Arizona, NAS5-02015, and JWST Program 3215. The research of CCW is supported by NOIRLab, which is managed by the Association of Universities for Research in Astronomy (AURA) under a cooperative agreement with the National Science Foundation. The FABLE simulations were performed on the DiRAC Darwin Supercomputer hosted by the University of Cambridge High Performance Computing Service (<http://www.hpc.cam.ac.uk/>), provided by Dell Inc. using Strategic Research Infrastructure Funding from the Higher Education Funding Council for England and funding from the Science and Technology Facilities Council; the COSMA Data Centric system at Durham University, operated by the Institute for Computational Cosmology on behalf of the STFC DiRAC HPC Facility. This equipment was funded by a BIS National E-infrastructure capital grant ST/K00042X/1, STFC capital grant ST/K00087X/1, DiRAC Operations grant ST/K003267/1 and Durham University. S.K. acknowledges support from St Catharine’s College through a Junior Research Fellowship. RS acknowledges support from the PRIN 2022 MUR project 2022CB3PJ3 - First Light And Galaxy aSsembly (FLAGS) funded by the European Union – Next Generation EU. AT and RV acknowledge support from the PRIN 2022 MUR project 2022935STW and 2023 INAF Theory Grant ”Theoretical models for Black Holes Archaeology”.

References

- [1] Harikane, Y., Zhang, Y., Nakajima, K., Ouchi, M., Isobe, Y., Ono, Y., Hatano, S., Xu, Y., Umeda, H.: A JWST/NIRSpec First Census of Broad-Line AGNs at $z=4-7$: Detection of 10 Faint AGNs with $M_{\text{BH}} \sim 10^6-10^8 M_{\text{sun}}$ and Their Host Galaxy Properties. arXiv e-prints, 2303–11946 (2023) <https://doi.org/10.48550/arXiv.2303.11946> [arXiv:2303.11946](https://arxiv.org/abs/2303.11946) [astro-ph.GA]
- [2] Maiolino, R., Scholtz, J., Curtis-Lake, E., Carniani, S., Baker, W., de Graaff, A., Tacchella, S., Übler, H., D’Eugenio, F., Witstok, J., Curti, M., Arribas, S., Bunker, A.J., Charlot, S., Chevallard, J., Eisenstein, D.J., Egami, E., Ji, Z., Jones, G.C., Lyu, J., Rawle, T., Robertson, B., Rujopakarn, W., Perna, M., Sun, F., Venturi, G., Williams, C.C., Willott, C.: JADES. The diverse population of infant Black Holes at $4 < z < 11$: merging, tiny, poor, but mighty. arXiv e-prints, 2308–01230 (2023) <https://doi.org/10.48550/arXiv.2308.01230> [arXiv:2308.01230](https://arxiv.org/abs/2308.01230)
- [3] Matthee, J., Naidu, R.P., Brammer, G., Chisholm, J., Eilers, A.-C., Goulding, A., Greene, J., Kashino, D., Labbe, I., Lilly, S.J., Mackenzie, R., Oesch, P.A., Weibel, A., Wuyts, S., Xiao, M., Bordoloi, R., Bouwens, R., van Dokkum, P., Illingworth, G., Kramarenko, I., Maseda, M.V., Mason, C., Meyer, R.A., Nelson, E.J., Reddy, N.A., Shivaei, I., Simcoe, R.A., Yue, M.: Little Red Dots: an abundant population of faint AGN at $z \sim 5$ revealed by the EIGER and FRESCO JWST surveys. arXiv e-prints, 2306–05448 (2023) <https://doi.org/10.48550/arXiv.2306.05448> [arXiv:2306.05448](https://arxiv.org/abs/2306.05448) [astro-ph.GA]

- [4] Übler, H., Maiolino, R., Curtis-Lake, E., Pérez-González, P.G., Curti, M., Perna, M., Arribas, S., Charlot, S., Marshall, M.A., D'Eugenio, F., Scholtz, J., Bunker, A., Carniani, S., Ferruit, P., Jakobsen, P., Rix, H.-W., Rodríguez Del Pino, B., Willott, C.J., Boeker, T., Cresci, G., Jones, G.C., Kumari, N., Rawle, T.: GA-NIFS: A massive black hole in a low-metallicity AGN at $z \sim 5.55$ revealed by JWST/NIRSpec IFS. *A&A* **677**, 145 (2023) <https://doi.org/10.1051/0004-6361/202346137> [arXiv:2302.06647](https://arxiv.org/abs/2302.06647) [astro-ph.GA]
- [5] Goulding, A.D., Greene, J.E., Setton, D.J., Labbe, I., Bezanson, R., Miller, T.B., Atek, H., Bogdán, Á., Brammer, G., Chemerynska, I., Cutler, S.E., Dayal, P., Fudamoto, Y., Fujimoto, S., Furtak, L.J., Kokorev, V., Khullar, G., Leja, J., Marchesini, D., Natarajan, P., Nelson, E., Oesch, P.A., Pan, R., Papovich, C., Price, S.H., van Dokkum, P., Wang, B., Weaver, J.R., Whitaker, K.E., Zitrin, A.: UNCOVER: The Growth of the First Massive Black Holes from JWST/NIRSpec-Spectroscopic Redshift Confirmation of an X-Ray Luminous AGN at $z = 10.1$. *ApJ* **955**(1), 24 (2023) <https://doi.org/10.3847/2041-8213/acf7c5> [arXiv:2308.02750](https://arxiv.org/abs/2308.02750) [astro-ph.GA]
- [6] Kokorev, V., Fujimoto, S., Labbe, I., Greene, J.E., Bezanson, R., Dayal, P., Nelson, E.J., Atek, H., Brammer, G., Caputi, K.I., Chemerynska, I., Cutler, S.E., Feldmann, R., Fudamoto, Y., Furtak, L.J., Goulding, A.D., de Graaff, A., Leja, J., Marchesini, D., Miller, T.B., Nanayakkara, T., Oesch, P.A., Pan, R., Price, S.H., Setton, D.J., Smit, R., Stefanon, M., Wang, B., Weaver, J.R., Whitaker, K.E., Williams, C.C., Zitrin, A.: UNCOVER: A NIRSpec Identification of a Broad-line AGN at $z = 8.50$. *ApJ* **957**(1), 7 (2023) <https://doi.org/10.3847/2041-8213/ad037a> [arXiv:2308.11610](https://arxiv.org/abs/2308.11610) [astro-ph.GA]
- [7] Übler, H., Maiolino, R., Pérez-González, P.G., D'Eugenio, F., Perna, M., Curti, M., Arribas, S., Bunker, A., Carniani, S., Charlot, S., Rodríguez Del Pino, B., Baker, W., Böker, T., Cresci, G., Dunlop, J., Grogin, N.A., Jones, G.C., Kumari, N., Lamperti, I., Laporte, N., Marshall, M.A., Mazzolari, G., Parlanti, E., Rawle, T., Scholtz, J., Venturi, G., Witstok, J.: GA-NIFS: JWST discovers an offset AGN 740 million years after the Big Bang. *arXiv e-prints*, 2312–03589 (2023) <https://doi.org/10.48550/arXiv.2312.03589> [arXiv:2312.03589](https://arxiv.org/abs/2312.03589) [astro-ph.GA]
- [8] Furtak, L.J., Labbé, I., Zitrin, A., Greene, J.E., Dayal, P., Chemerynska, I., Kokorev, V., Miller, T.B., Goulding, A.D., Bezanson, R., Brammer, G.B., Cutler, S.E., Leja, J., Pan, R., Price, S.H., Wang, B., Weaver, J.R., Whitaker, K.E., Atek, H., Bogdán, Á., Charlot, S., Curtis-Lake, E., van Dokkum, P., Endsley, R., Fudamoto, Y., Fujimoto, S., de Graaff, A., Glazebrook, K., Juneau, S., Marchesini, D., Masada, M.V., Nelson, E., Oesch, P.A., Plat, A., Setton, D.J., Stark, D.P., Williams, C.C.: A supermassive black hole in the early universe growing in the shadows. *arXiv e-prints*, 2308–05735 (2023) <https://doi.org/10.48550/arXiv.2308.05735> [arXiv:2308.05735](https://arxiv.org/abs/2308.05735) [astro-ph.GA]
- [9] Maiolino, R., Scholtz, J., Witstok, J., Carniani, S., D'Eugenio, F., de Graaff,

- A., Uebler, H., Tacchella, S., Curtis-Lake, E., Arribas, S., Bunker, A., Charlot, S., Chevallard, J., Curti, M., Looser, T.J., Maseda, M.V., Rawle, T., Rodríguez Del Pino, B., Willott, C.J., Egami, E., Eisenstein, D., Hainline, K., Robertson, B., Williams, C.C., Willmer, C.N.A., Baker, W.M., Boyett, K., DeCoursey, C., Fabian, A.C., Helton, J.M., Ji, Z., Jones, G.C., Kumari, N., Laporte, N., Nelson, E., Perna, M., Sandles, L., Shivaiei, I., Sun, F.: A small and vigorous black hole in the early Universe. arXiv e-prints, 2305–12492 (2023) <https://doi.org/10.48550/arXiv.2305.12492> [astro-ph.GA]
- [10] Übler, H., Maiolino, R., Pérez-González, P.G., D'Eugenio, F., Perna, M., Curti, M., Arribas, S., Bunker, A., Carniani, S., Charlot, S., Rodríguez Del Pino, B., Baker, W., Böker, T., Cresci, G., Dunlop, J., Grogin, N.A., Jones, G.C., Kumari, N., Lamperti, I., Laporte, N., Marshall, M.A., Mazzolari, G., Parlanti, E., Rawle, T., Scholtz, J., Venturi, G., Witstok, J.: GA-NIFS: JWST discovers an offset AGN 740 million years after the Big Bang. arXiv e-prints, 2312–03589 (2023) <https://doi.org/10.48550/arXiv.2312.03589> [astro-ph.GA]
- [11] Schneider, R., Valiante, R., Trinca, A., Graziani, L., Volonteri, M., Maiolino, R.: Are we surprised to find SMBHs with JWST at $z \geq 9$? MNRAS **526**(3), 3250–3261 (2023) <https://doi.org/10.1093/mnras/stad2503> arXiv:2305.12504 [astro-ph.GA]
- [12] Trinca, A., Schneider, R., Valiante, R., Graziani, L., Zappacosta, L., Shankar, F.: The low-end of the black hole mass function at cosmic dawn. MNRAS **511**(1), 616–640 (2022) <https://doi.org/10.1093/mnras/stac062> arXiv:2201.02630 [astro-ph.GA]
- [13] Volonteri, M., Habouzit, M., Colpi, M.: What if young $z \lesssim 9$ JWST galaxies hosted massive black holes? MNRAS **521**(1), 241–250 (2023) <https://doi.org/10.1093/mnras/stad499> arXiv:2212.04710 [astro-ph.GA]
- [14] Pacucci, F., Nguyen, B., Carniani, S., Maiolino, R., Fan, X.: JWST CEERS and JADES Active Galaxies at $z = 4-7$ Violate the Local $M_{\text{BH}}-M_{\text{star}}$ Relation at $z \gtrsim 3$: Implications for Low-mass Black Holes and Seeding Models. ApJ **957**(1), 3 (2023) <https://doi.org/10.3847/2041-8213/ad0158> arXiv:2308.12331 [astro-ph.GA]
- [15] Bennett, J.S., Sijacki, D., Costa, T., Laporte, N., Witten, C.: The growth of the gargantuan black holes powering high-redshift quasars and their impact on the formation of early galaxies and protoclusters. MNRAS **527**(1), 1033–1054 (2024) <https://doi.org/10.1093/mnras/stad3179> arXiv:2305.11932 [astro-ph.GA]
- [16] Zhang, H., Behroozi, P., Volonteri, M., Silk, J., Fan, X., Aird, J., Yang, J., Hopkins, P.F.: TRINITY II: The luminosity-dependent bias of the supermassive black hole mass-galaxy mass relation for bright quasars at $z = 6$. MNRAS **523**(1), 69–74 (2023) <https://doi.org/10.1093/mnras/slad060> arXiv:2303.08150 [astro-ph.GA]
- [17] Koudmani, S., Somerville, R.S., Sijacki, D., Bourne, M.A., Jiang, Y.-F., Profit,

- K.: A unified accretion disc model for supermassive black holes in galaxy formation simulations: method and implementation. arXiv e-prints, 2312–08428 (2023) <https://doi.org/10.48550/arXiv.2312.08428> arXiv:2312.08428 [astro-ph.GA]
- [18] Reines, A.E., Greene, J.E., Geha, M.: Dwarf Galaxies with Optical Signatures of Active Massive Black Holes. *ApJ* **775**(2), 116 (2013) <https://doi.org/10.1088/0004-637X/775/2/116> arXiv:1308.0328 [astro-ph.CO]
- [19] Reines, A.E., Volonteri, M.: Relations between Central Black Hole Mass and Total Galaxy Stellar Mass in the Local Universe. *ApJ* **813**(2), 82 (2015) <https://doi.org/10.1088/0004-637X/813/2/82> arXiv:1508.06274 [astro-ph.GA]
- [20] Stern, J., Laor, A.: Type 1 AGN at low z - I. Emission properties. *MNRAS* **423**(1), 600–631 (2012) <https://doi.org/10.1111/j.1365-2966.2012.20901.x> arXiv:1203.3158 [astro-ph.CO]
- [21] Abuter, R., Allouche, F., Amorim, A., Bailet, C., Berdeu, A., Berger, J.-P., Berio, P., Biglioli, A., Boebion, O., Bolzer, M.-L., Bonnet, H., Bourdarot, G., Bourget, P., Brandner, W., Cao, Y., Conzelmann, R., Comin, M., Clénet, Y., Courtney-Barrer, B., Davies, R., Defrère, D., Delboulbé, A., Delplancke-Ströbele, F., Dembet, R., Dexter, J., de Zeeuw, P.T., Drescher, A., Eckart, A., Édouard, C., Eisenhauer, F., Fabricius, M., Feuchtgruber, H., Finger, G., Förster Schreiber, N.M., Garcia, P., Garcia Lopez, R., Gao, F., Gendron, E., Genzel, R., Gil, J.P., Gillessen, S., Gomes, T., Gonté, F., Gouvret, C., Guajardo, P., Guieu, S., Hackenberg, W., Haddad, N., Hartl, M., Haubois, X., Haußmann, F., Heißel, G., Henning, T., Hippler, S., Hönig, S.F., Horrobin, M., Hubin, N., Jacqmart, E., Jocu, L., Kaufer, A., Kervella, P., Kolb, J., Korhonen, H., Lacour, S., Lagarde, S., Lai, O., Lapeyrère, V., Laugier, R., Le Bouquin, J.-B., Leftley, J., Léna, P., Lewis, S., Liu, D., Lopez, B., Lutz, D., Magnard, Y., Mang, F., Marcotto, A., Maurel, D., Mérand, A., Millour, F., More, N., Netzer, H., Nowacki, H., Nowak, M., Oberti, S., Ott, T., Pallanca, L., Paumard, T., Perraut, K., Perrin, G., Petrov, R., Pfuhl, O., Pourré, N., Rabien, S., Rau, C., Riquelme, M., Robbe-Dubois, S., Rochat, S., Salman, M., Sanchez-Bermudez, J., Santos, D.J.D., Scheithauer, S., Schöller, M., Schubert, J., Schuhler, N., Shangguan, J., Shchekaturov, P., Shimizu, T.T., Sevin, A., Soulez, F., Spang, A., Stadler, E., Sternberg, A., Straubmeier, C., Sturm, E., Sykes, C., Tacconi, L.J., Tristram, K.R.W., Vincent, F., von Fellenberg, S., Uysal, S., Widmann, F., Wierprecht, E., Wierzorrek, E., Woillez, J., Zins, G.: A dynamical measure of the black hole mass in a quasar 11 billion years ago. arXiv e-prints, 2401–14567 (2024) <https://doi.org/10.48550/arXiv.2401.14567> arXiv:2401.14567 [astro-ph.GA]
- [22] Carnall, A.C., McLure, R.J., Dunlop, J.S., Davé, R.: Inferring the star formation histories of massive quiescent galaxies with BAGPIPES: evidence for multiple quenching mechanisms. *MNRAS* **480**(4), 4379–4401 (2018) <https://doi.org/10.1093/mnras/sty2169> arXiv:1712.04452 [astro-ph.GA]
- [23] Johnson, B.D., Leja, J., Conroy, C., Speagle, J.S.: Stellar Population Inference

- with Prospector. *ApJS* **254**(2), 22 (2021) <https://doi.org/10.3847/1538-4365/abef67> [arXiv:2012.01426](https://arxiv.org/abs/2012.01426) [astro-ph.GA]
- [24] Popesso, P., Concas, A., Cresci, G., Belli, S., Rodighiero, G., Inami, H., Dickinson, M., Ilbert, O., Pannella, M., Elbaz, D.: The main sequence of star-forming galaxies across cosmic times. *MNRAS* **519**(1), 1526–1544 (2023) <https://doi.org/10.1093/mnras/stac3214> [arXiv:2203.10487](https://arxiv.org/abs/2203.10487) [astro-ph.GA]
- [25] Laporte, N., Ellis, R.S., Witten, C.E.C., Roberts-Borsani, G.: Resolving ambiguities in the inferred star formation histories of intense [O III] emitters in the reionization Era. *MNRAS* **523**(2), 3018–3024 (2023) <https://doi.org/10.1093/mnras/stad1597> [arXiv:2212.05072](https://arxiv.org/abs/2212.05072) [astro-ph.GA]
- [26] Leethochawalit, N., Trenti, M., Santini, P., Yang, L., Merlin, E., Castellano, M., Fontana, A., Treu, T., Mason, C., Glazebrook, K., Jones, T., Vulcani, B., Nanayakkara, T., Marchesini, D., Mascia, S., Morishita, T., Roberts-Borsani, G., Bonchi, A., Paris, D., Boyett, K., Strait, V., Calabrò, A., Pentericci, L., Bradac, M., Wang, X., Scarlata, C.: Early Results from GLASS-JWST. X. Rest-frame UV-optical Properties of Galaxies at $7 \lesssim z \lesssim 9$. *ApJ* **942**(2), 26 (2023) <https://doi.org/10.3847/2041-8213/ac959b> [arXiv:2207.11135](https://arxiv.org/abs/2207.11135) [astro-ph.GA]
- [27] Laporte, N., Zitrin, A., Dole, H., Roberts-Borsani, G., Furtak, L.J., Witten, C.: A lensed protocluster candidate at $z = 7.66$ identified in JWST observations of the galaxy cluster SMACS0723–7327. *A&A* **667**, 3 (2022) <https://doi.org/10.1051/0004-6361/202244719> [arXiv:2208.04930](https://arxiv.org/abs/2208.04930) [astro-ph.GA]
- [28] Roberts-Borsani, G., Morishita, T., Treu, T., Leethochawalit, N., Trenti, M.: The Physical Properties of Luminous $z \gtrsim 8$ Galaxies and Implications for the Cosmic Star Formation Rate Density from 0.35 deg² of (Pure-)Parallel HST Observations. *ApJ* **927**(2), 236 (2022) <https://doi.org/10.3847/1538-4357/ac4803> [arXiv:2106.06544](https://arxiv.org/abs/2106.06544) [astro-ph.GA]
- [29] Topping, M.W., Stark, D.P., Endsley, R., Bouwens, R.J., Schouws, S., Smit, R., Stefanon, M., Inami, H., Bowler, R.A.A., Oesch, P., Gonzalez, V., Dayal, P., da Cunha, E., Algera, H., van der Werf, P., Pallottini, A., Barrufet, L., Schneider, R., De Looze, I., Sommovigo, L., Whitler, L., Graziani, L., Fudamoto, Y., Ferrara, A.: The ALMA REBELS Survey: specific star formation rates in the reionization era. *MNRAS* **516**(1), 975–991 (2022) <https://doi.org/10.1093/mnras/stac2291> [arXiv:2203.07392](https://arxiv.org/abs/2203.07392) [astro-ph.GA]
- [30] Carnall, A.C., McLure, R.J., Dunlop, J.S., McLeod, D.J., Wild, V., Cullen, F., Magee, D., Begley, R., Cimatti, A., Donnan, C.T., Hamadouche, M.L., Jewell, S.M., Walker, S.: A massive quiescent galaxy at redshift 4.658. *Nature* **619**(7971), 716–719 (2023) <https://doi.org/10.1038/s41586-023-06158-6> [arXiv:2301.11413](https://arxiv.org/abs/2301.11413) [astro-ph.GA]
- [31] Mazzucchelli, C., Bischetti, M., D’Odorico, V., Feruglio, C., Schindler, J.-T.,

- Onoue, M., Bañados, E., Becker, G.D., Bian, F., Carniani, S., Decarli, R., Eilers, A.-C., Farina, E.P., Gallerani, S., Lai, S., Meyer, R.A., Rojas-Ruiz, S., Satyavolu, S., Venemans, B.P., Wang, F., Yang, J., Zhu, Y.: XQR-30: Black hole masses and accretion rates of 42 $z \gtrsim 6$ quasars. *A&A* **676**, 71 (2023) <https://doi.org/10.1051/0004-6361/202346317> arXiv:2306.16474 [astro-ph.GA]
- [32] Zappacosta, L., Piconcelli, E., Fiore, F., Saccheo, I., Valiante, R., Vignali, C., Vito, F., Volonteri, M., Bischetti, M., Comastri, A., Done, C., Elvis, M., Giallongo, E., La Franca, F., Lanzuisi, G., Laurenti, M., Miniutti, G., Bongiorno, A., Brusa, M., Civano, F., Carniani, S., D’Odorico, V., Feruglio, C., Gallerani, S., Gilli, R., Grazian, A., Guainazzi, M., Marinucci, A., Menci, N., Middei, R., Nicastro, F., Puccetti, S., Tombesi, F., Tortosa, A., Testa, V., Vietri, G., Cristiani, S., Haardt, F., Maiolino, R., Schneider, R., Tripodi, R., Vallini, L., Vanzella, E.: HYPERluminous quasars at the Epoch of ReionizatION (HYPERION): A new regime for the X-ray nuclear properties of the first quasars. *A&A* **678**, 201 (2023) <https://doi.org/10.1051/0004-6361/202346795> arXiv:2305.02347 [astro-ph.GA]
- [33] Stone, M.A., Lyu, J., Rieke, G.H., Alberts, S., Hainline, K.N.: Undermassive Host Galaxies of Five $z \sim 6$ Luminous Quasars Detected with JWST. arXiv e-prints, 2310–18395 (2023) <https://doi.org/10.48550/arXiv.2310.18395> arXiv:2310.18395 [astro-ph.GA]
- [34] Ding, X., Onoue, M., Silverman, J.D., Matsuoka, Y., Izumi, T., Strauss, M.A., Jahnke, K., Phillips, C.L., Li, J., Volonteri, M., Haiman, Z., Andika, I.T., Aoki, K., Baba, S., Bieri, R., Bosman, S.E.I., Bottrell, C., Eilers, A.-C., Fujimoto, S., Habouzit, M., Imanishi, M., Inayoshi, K., Iwasawa, K., Kashikawa, N., Kawaguchi, T., Kohno, K., Lee, C.-H., Lupi, A., Lyu, J., Nagao, T., Overzier, R., Schindler, J.-T., Schramm, M., Shimasaku, K., Toba, Y., Trakhtenbrot, B., Trebitsch, M., Treu, T., Umehata, H., Venemans, B.P., Vestergaard, M., Walter, F., Wang, F., Yang, J.: Detection of stellar light from quasar host galaxies at redshifts above 6. *Nature* **621**(7977), 51–55 (2023) <https://doi.org/10.1038/s41586-023-06345-5> arXiv:2211.14329 [astro-ph.GA]
- [35] Yue, M., Eilers, A.-C., Simcoe, R.A., Mackenzie, R., Matthee, J., Kashino, D., Bordoloi, R., Lilly, S.J., Naidu, R.P.: EIGER V. Characterizing the Host Galaxies of Luminous Quasars at *zrsim6*. arXiv e-prints, 2309–04614 (2023) <https://doi.org/10.48550/arXiv.2309.04614> arXiv:2309.04614 [astro-ph.GA]
- [36] Bogdán, Á., Kovács, O.E., Jones, C., Forman, W.R., Kraft, R.P., Strait, V., Coe, D., Bradač, M.: Exploring Gravitationally Lensed $z \gtrsim 6$ X-Ray Active Galactic Nuclei Behind the RELICS Clusters. *ApJ* **927**(1), 34 (2022) <https://doi.org/10.3847/1538-4357/ac4ae5> arXiv:2111.03669 [astro-ph.GA]
- [37] Zhang, H., Behroozi, P., Volonteri, M., Silk, J., Fan, X., Aird, J., Yang, J., Wang, F., Hopkins, P.F.: TRINITY IV: Predictions for Supermassive Black Holes at *zrsim7*. arXiv e-prints, 2309–07210 (2023) <https://doi.org/10.48550/arXiv.2309.07210>

07210 arXiv:2309.07210 [astro-ph.GA]

- [38] Li, J., Silverman, J.D., Shen, Y., Volonteri, M., Jahnke, K., Zhuang, M.-Y., Scoggins, M.T., Ding, X., Harikane, Y., Onoue, M., Tanaka, T.S.: Tip of the iceberg: overmassive black holes at $4 < z < 7$ found by JWST are not inconsistent with the local $\mathcal{M}_{\text{BH}}\text{-}\mathcal{M}_{\star}$ relation. arXiv e-prints, 2403–00074 (2024) [arXiv:2403.00074](https://arxiv.org/abs/2403.00074) [astro-ph.GA]
- [39] Bennert, V.N., Treu, T., Ding, X., Stomberg, I., Birrer, S., Snyder, T., Malkan, M.A., Stephens, A.W., Auger, M.W.: A Local Baseline of the Black Hole Mass Scaling Relations for Active Galaxies. IV. Correlations Between M_{BH} and Host Galaxy σ , Stellar Mass, and Luminosity. *ApJ* **921**(1), 36 (2021) <https://doi.org/10.3847/1538-4357/ac151a> arXiv:2101.10355 [astro-ph.GA]
- [40] Kormendy, J., Ho, L.C.: Coevolution (Or Not) of Supermassive Black Holes and Host Galaxies. *ARA&A* **51**(1), 511–653 (2013) <https://doi.org/10.1146/annurev-astro-082708-101811> arXiv:1304.7762 [astro-ph.CO]
- [41] Trinca, A., Schneider, R., Maiolino, R., Valiante, R., Graziani, L., Volonteri, M.: Seeking the growth of the first black hole seeds with JWST. *MNRAS* **519**(3), 4753–4764 (2023) <https://doi.org/10.1093/mnras/stac3768> arXiv:2211.01389 [astro-ph.GA]
- [42] Dayal, P., Volonteri, M., Greene, J.E., Kokorev, V., Goulding, A.D., Williams, C.C., Furtak, L.J., Zitrin, A., Atek, H., Chemerynska, I., Feldmann, R., Glazebrook, K., Labbe, I., Nanayakkara, T., Oesch, P.A., Weaver, J.R.: UNCOVERing the contribution of black holes to reionization in the JWST era. arXiv e-prints, 2401–11242 (2024) <https://doi.org/10.48550/arXiv.2401.11242> arXiv:2401.11242 [astro-ph.GA]
- [43] Lupi, A., Quadri, G., Volonteri, M., Colpi, M., Regan, J.A.: Sustained super-Eddington accretion in high-redshift quasars. arXiv e-prints, 2312–08422 (2023) <https://doi.org/10.48550/arXiv.2312.08422> arXiv:2312.08422 [astro-ph.GA]
- [44] Pezzulli, E., Valiante, R., Schneider, R.: Super-Eddington growth of the first black holes. *MNRAS* **458**(3), 3047–3059 (2016) <https://doi.org/10.1093/mnras/stw505> arXiv:1603.00475 [astro-ph.GA]
- [45] Henden, N.A., Puchwein, E., Shen, S., Sijacki, D.: The FABLE simulations: a feedback model for galaxies, groups, and clusters. *MNRAS* **479**(4), 5385–5412 (2018)
- [46] Mezcua, M., Siudek, M., Suh, H., Valiante, R., Spinoso, D., Bonoli, S.: Overmassive Black Holes in Dwarf Galaxies Out to $z < 0.9$ in the VIPERS Survey. *ApJ* **943**(1), 5 (2023) <https://doi.org/10.3847/2041-8213/aca25> arXiv:2212.14057 [astro-ph.GA]

- [47] Peng, Y.-j., Renzini, A.: Disc growth and quenching. *MNRAS* **491**(1), 51–55 (2020) <https://doi.org/10.1093/mnras/slz163> arXiv:1910.10446 [astro-ph.GA]
- [48] Dubois, Y., Pichon, C., Haehnelt, M., Kimm, T., Slyz, A., Devriendt, J., Pogosyan, D.: Feeding compact bulges and supermassive black holes with low angular momentum cosmic gas at high redshift. *MNRAS* **423**(4), 3616–3630 (2012) <https://doi.org/10.1111/j.1365-2966.2012.21160.x> 1002/asna.19141990903 arXiv:1112.2479 [astro-ph.CO]
- [49] Tacchella, S., Carollo, C.M., Renzini, A., Förster Schreiber, N.M., Lang, P., Wuyts, S., Cresci, G., Dekel, A., Genzel, R., Lilly, S.J., Mancini, C., Newman, S., Onodera, M., Shapley, A., Tacconi, L., Woo, J., Zamorani, G.: Evidence for mature bulges and an inside-out quenching phase 3 billion years after the Big Bang. *Science* **348**(6232), 314–317 (2015) <https://doi.org/10.1126/science.1261094> arXiv:1504.04021 [astro-ph.GA]
- [50] Baker, W.M., Tacchella, S., Johnson, B.D., Nelson, E., Suess, K.A., D’Eugenio, F., Curti, M., de Graaff, A., Ji, Z., Maiolino, R., Robertson, B., Scholtz, J., Alberts, S., Arribas, S., Boyett, K., Bunker, A.J., Carniani, S., Charlot, S., Chen, Z., Chevallard, J., Curtis-Lake, E., Danhaive, A.L., DeCoursey, C., Egami, E., Eisenstein, D.J., Endsley, R., Hausen, R., Helton, J.M., Kumari, N., Looser, T.J., Maseda, M.V., Puskás, D., Rieke, M., Sandles, L., Sun, F., Übler, H., Williams, C.C., Willmer, C.N.A., Witstok, J.: Inside-out growth in the early Universe: a core in a vigorously star-forming disc. arXiv e-prints, 2306–02472 (2023) <https://doi.org/10.48550/arXiv.2306.02472> arXiv:2306.02472 [astro-ph.GA]
- [51] Bunker, A.J., Cameron, A.J., Curtis-Lake, E., Jakobsen, P., Carniani, S., Curti, M., Witstok, J., Maiolino, R., D’Eugenio, F., Looser, T.J., Willott, C., Bonaventura, N., Hainline, K., Uebler, H., Willmer, C.N.A., Saxena, A., Smit, R., Alberts, S., Arribas, S., Baker, W.M., Baum, S., Bhatawdekar, R., Bowler, R.A.A., Boyett, K., Charlot, S., Chen, Z., Chevallard, J., Circosta, C., DeCoursey, C., de Graaff, A., Egami, E., Eisenstein, D.J., Endsley, R., Ferruit, P., Giardino, G., Hausen, R., Helton, J.M., Hviding, R.E., Ji, Z., Johnson, B.D., Jones, G.C., Kumari, N., Laseter, I., Luetzgendorf, N., Maseda, M.V., Nelson, E., Parlanti, E., Perna, M., Rawle, T., Rix, H.-W., Rieke, M., Robertson, B., Rodriguez Del Pino, B., Sandles, L., Scholtz, J., Sharpe, K., Skarbinski, M., Stark, D.P., Sun, F., Tacchella, S., Topping, M.W., Villanueva, N.C., Wallace, I.E.B., Williams, C.C., Woodrum, C.: JADES NIRSpec Initial Data Release for the Hubble Ultra Deep Field: Redshifts and Line Fluxes of Distant Galaxies from the Deepest JWST Cycle 1 NIRSpec Multi-Object Spectroscopy. arXiv e-prints, 2306–02467 (2023) <https://doi.org/10.48550/arXiv.2306.02467> arXiv:2306.02467 [astro-ph.GA]
- [52] Eisenstein, D.J., Willott, C., Alberts, S., Arribas, S., Bonaventura, N., Bunker, A.J., Cameron, A.J., Carniani, S., Charlot, S., Curtis-Lake, E., D’Eugenio, F., Endsley, R., Ferruit, P., Giardino, G., Hainline, K., Hausen, R., Jakobsen, P., Johnson, B.D., Maiolino, R., Rieke, M., Rieke, G., Rix, H.-W., Robertson, B.,

- Stark, D.P., Tacchella, S., Williams, C.C., Willmer, C.N.A., Baker, W.M., Baum, S., Bhatawdekar, R., Boyett, K., Chen, Z., Chevallard, J., Circosta, C., Curti, M., Danhaive, A.L., DeCoursey, C., de Graaff, A., Dressler, A., Egami, E., Helton, J.M., Hviding, R.E., Ji, Z., Jones, G.C., Kumari, N., Lützgendorf, N., Laseter, I., Looser, T.J., Lyu, J., Maseda, M.V., Nelson, E., Parlanti, E., Perna, M., Puskás, D., Rawle, T., Rodríguez Del Pino, B., Sandles, L., Saxena, A., Scholtz, J., Sharpe, K., Shivaiei, I., Silcock, M.S., Simmonds, C., Skarbinski, M., Smit, R., Stone, M., Suess, K.A., Sun, F., Tang, M., Topping, M.W., Übler, H., Villanueva, N.C., Wallace, I.E.B., Whitler, L., Witstok, J., Woodrum, C.: Overview of the JWST Advanced Deep Extragalactic Survey (JADES). arXiv e-prints, 2306–02465 (2023) <https://doi.org/10.48550/arXiv.2306.02465> arXiv:2306.02465 [astro-ph.GA]
- [53] Bunker, A.J., Saxena, A., Cameron, A.J., Willott, C.J., Curtis-Lake, E., Jakobsen, P., Carniani, S., Smit, R., Maiolino, R., Witstok, J., Curti, M., D’Eugenio, F., Jones, G.C., Ferruit, P., Arribas, S., Charlot, S., Chevallard, J., Giardino, G., de Graaff, A., Looser, T.J., Lützgendorf, N., Maseda, M.V., Rawle, T., Rix, H.-W., Del Pino, B.R., Alberts, S., Egami, E., Eisenstein, D.J., Endsley, R., Hainline, K., Hausen, R., Johnson, B.D., Rieke, G., Rieke, M., Robertson, B.E., Shivaiei, I., Stark, D.P., Sun, F., Tacchella, S., Tang, M., Williams, C.C., Willmer, C.N.A., Baker, W.M., Baum, S., Bhatawdekar, R., Bowler, R., Boyett, K., Chen, Z., Circosta, C., Helton, J.M., Ji, Z., Kumari, N., Lyu, J., Nelson, E., Parlanti, E., Perna, M., Sandles, L., Scholtz, J., Suess, K.A., Topping, M.W., Übler, H., Wallace, I.E.B., Whitler, L.: JADES NIRSpectroscopy of GN-z11: Lyman- α emission and possible enhanced nitrogen abundance in a $z = 10.60$ luminous galaxy. *A&A* **677**, 88 (2023) <https://doi.org/10.1051/0004-6361/202346159> arXiv:2302.07256 [astro-ph.GA]
- [54] Carniani, S., Venturi, G., Parlanti, E., de Graaff, A., Maiolino, R., Arribas, S., Bonaventura, N., Boyett, K., Bunker, A.J., Cameron, A.J., Charlot, S., Chevallard, J., Curti, M., Curtis-Lake, E., Eisenstein, D.J., Giardino, G., Hausen, R., Kumari, N., Maseda, M.V., Nelson, E., Perna, M., Rix, H.-W., Robertson, B., Rodríguez Del Pino, B., Sandles, L., Scholtz, J., Simmonds, C., Smit, R., Tacchella, S., Übler, H., Williams, C.C., Willott, C., Witstok, J.: JADES: The incidence rate and properties of galactic outflows in low-mass galaxies across $3 < z < 9$. arXiv e-prints, 2306–11801 (2023) <https://doi.org/10.48550/arXiv.2306.11801> arXiv:2306.11801 [astro-ph.GA]
- [55] Robertson, B.E., Tacchella, S., Johnson, B.D., Hainline, K., Whitler, L., Eisenstein, D.J., Endsley, R., Rieke, M., Stark, D.P., Alberts, S., Dressler, A., Egami, E., Hausen, R., Rieke, G., Shivaiei, I., Williams, C.C., Willmer, C.N.A., Arribas, S., Bonaventura, N., Bunker, A., Cameron, A.J., Carniani, S., Charlot, S., Chevallard, J., Curti, M., Curtis-Lake, E., D’Eugenio, F., Jakobsen, P., Looser, T.J., Lützgendorf, N., Maiolino, R., Maseda, M.V., Rawle, T., Rix, H.-W., Smit, R., Übler, H., Willott, C., Witstok, J., Baum, S., Bhatawdekar, R., Boyett, K., Chen, Z., de Graaff, A., Florian, M., Helton, J.M., Hviding, R.E., Ji, Z.,

- Kumari, N., Lyu, J., Nelson, E., Sandles, L., Saxena, A., Suess, K.A., Sun, F., Topping, M., Wallace, I.E.B.: Identification and properties of intense star-forming galaxies at redshifts $z < 10$. *Nature Astronomy* **7**, 611–621 (2023) <https://doi.org/10.1038/s41550-023-01921-1> arXiv:2212.04480 [astro-ph.GA]
- [56] Tacchella, S., Eisenstein, D.J., Hainline, K., Johnson, B.D., Baker, W.M., Helton, J.M., Robertson, B., Suess, K.A., Chen, Z., Nelson, E., Puskás, D., Sun, F., Alberts, S., Egami, E., Hausen, R., Rieke, G., Rieke, M., Shivaiei, I., Williams, C.C., Willmer, C.N.A., Bunker, A., Cameron, A.J., Carniani, S., Charlot, S., Curti, M., Curtis-Lake, E., Looser, T.J., Maiolino, R., Maseda, M.V., Rawle, T., Rix, H.-W., Smit, R., Übler, H., Willott, C., Witstok, J., Baum, S., Bhatawdekar, R., Boyett, K., Danhaive, A.L., de Graaff, A., Endsley, R., Ji, Z., Lyu, J., Sandles, L., Saxena, A., Scholtz, J., Topping, M.W., Whitler, L.: JADES Imaging of GN-z11: Revealing the Morphology and Environment of a Luminous Galaxy 430 Myr after the Big Bang. *ApJ* **952**(1), 74 (2023) <https://doi.org/10.3847/1538-4357/acdbc6> arXiv:2302.07234 [astro-ph.GA]
- [57] Bushouse, H., Eisenhamer, J., Dencheva, N., Davies, J., Greenfield, P., Morrison, J., Hodge, P., Simon, B., Grumm, D., Droettboom, M., Slavich, E., Sosey, M., Pauly, T., Miller, T., Jedrzejewski, R., Hack, W., Davis, D., Crawford, S., Law, D., Gordon, K., Regan, M., Cara, M., MacDonald, K., Bradley, L., Shanahan, C., Jamieson, W., Teodoro, M., Williams, T.: JWST Calibration Pipeline. <https://doi.org/10.5281/zenodo.7229890> . <https://doi.org/10.5281/zenodo.7229890>
- [58] Wang, W., Liu, X.-W., Zhang, Y., Barlow, M.J.: A reexamination of electron density diagnostics for ionized gaseous nebulae. *A&A* **427**, 873–886 (2004) <https://doi.org/10.1051/0004-6361:20041470> arXiv:astro-ph/0408040 [astro-ph]
- [59] Foreman-Mackey, D., Hogg, D.W., Lang, D., Goodman, J.: emcee: The MCMC Hammer. *PASP* **125**(925), 306 (2013) <https://doi.org/10.1086/670067> arXiv:1202.3665 [astro-ph.IM]
- [60] Zhang, X.: Are There Higher Electron Densities in Narrow Emission Line Regions of Type-1 AGNs than in Type-2 AGNs? *ApJ* **960**(2), 108 (2024) <https://doi.org/10.3847/1538-4357/ad029a> arXiv:2309.00852 [astro-ph.GA]
- [61] Dors, O.L., Freitas-Lemes, P., Amôres, E.B., Pérez-Montero, E., Cardaci, M.V., Hägele, G.F., Armah, M., Krabbe, A.C., Faúndez-Abans, M.: Chemical abundances of Seyfert 2 AGNs - I. Comparing oxygen abundances from distinct methods using SDSS. *MNRAS* **492**(1), 468–479 (2020) <https://doi.org/10.1093/mnras/stz3492> arXiv:1912.04236 [astro-ph.GA]
- [62] Nakajima, K., Ouchi, M., Isobe, Y., Harikane, Y., Zhang, Y., Ono, Y., Umeda, H., Oguri, M.: JWST Census for the Mass-Metallicity Star Formation Relations at $z = 4-10$ with Self-consistent Flux Calibration and Proper Metallicity Calibrators. *ApJS* **269**(2), 33 (2023) <https://doi.org/10.3847/1538-4365/acd556> arXiv:2301.12825 [astro-ph.GA]

- [63] Curti, M., Maiolino, R., Curtis-Lake, E., Chevallard, J., Carniani, S., D'Eugenio, F., Looser, T.J., Scholtz, J., Charlot, S., Cameron, A., Übler, H., Witstok, J., Boyett, K., Laseter, I., Sandles, L., Arribas, S., Bunker, A., Giardino, G., Maseda, M.V., Rawle, T., Rodríguez Del Pino, B., Smit, R., Willott, C.J., Eisenstein, D.J., Hausen, R., Johnson, B., Rieke, M., Robertson, B., Tacchella, S., Williams, C.C., Willmer, C., Baker, W.M., Bhatawdekar, R., Egami, E., Helton, J.M., Ji, Z., Kumari, N., Perna, M., Shivaiei, I., Sun, F.: JADES: Insights on the low-mass end of the mass–metallicity–star-formation rate relation at $3 < z < 10$ from deep JWST/NIRSpec spectroscopy. arXiv e-prints, 2304–08516 (2023) <https://doi.org/10.48550/arXiv.2304.08516> arXiv:2304.08516 [astro-ph.GA]
- [64] Gilli, R., Norman, C., Calura, F., Vito, F., Decarli, R., Marchesi, S., Iwasawa, K., Comastri, A., Lanzuisi, G., Pozzi, F., D'Amato, Q., Vignali, C., Brusa, M., Mignoli, M., Cox, P.: Supermassive black holes at high redshift are expected to be obscured by their massive host galaxies' interstellar medium. *A&A* **666**, 17 (2022) <https://doi.org/10.1051/0004-6361/202243708> arXiv:2206.03508 [astro-ph.GA]
- [65] Richards, G.T., Hall, P.B., Vanden Berk, D.E., Strauss, M.A., Schneider, D.P., Weinstein, M.A., Reichard, T.A., York, D.G., Knapp, G.R., Fan, X., Ivezić, Ž., Brinkmann, J., Budavári, T., Csabai, I., Nichol, R.C.: Red and Reddened Quasars in the Sloan Digital Sky Survey. *AJ* **126**(3), 1131–1147 (2003) <https://doi.org/10.1086/377014> arXiv:astro-ph/0305305 [astro-ph]
- [66] Reichard, T.A., Richards, G.T., Hall, P.B., Schneider, D.P., Vanden Berk, D.E., Fan, X., York, D.G., Knapp, G.R., Brinkmann, J.: Continuum and Emission-Line Properties of Broad Absorption Line Quasars. *AJ* **126**(6), 2594–2607 (2003) <https://doi.org/10.1086/379293> arXiv:astro-ph/0308508 [astro-ph]
- [67] Johnson, B.D., Leja, J., Conroy, C., Speagle, J.S.: Stellar Population Inference with Prospector. *ApJS* **254**(2), 22 (2021) <https://doi.org/10.3847/1538-4365/abef67> arXiv:2012.01426 [astro-ph.GA]
- [68] Conroy, C., Gunn, J.E., White, M.: The Propagation of Uncertainties in Stellar Population Synthesis Modeling. I. The Relevance of Uncertain Aspects of Stellar Evolution and the Initial Mass Function to the Derived Physical Properties of Galaxies. *ApJ* **699**(1), 486–506 (2009) <https://doi.org/10.1088/0004-637X/699/1/486> arXiv:0809.4261 [astro-ph]
- [69] Choi, J., Dotter, A., Conroy, C., Cantiello, M., Paxton, B., Johnson, B.D.: Mesa Isochrones and Stellar Tracks (MIST). I. Solar-scaled Models. *ApJ* **823**(2), 102 (2016) <https://doi.org/10.3847/0004-637X/823/2/102> arXiv:1604.08592 [astro-ph.SR]
- [70] Byler, N., Dalcanton, J.J., Conroy, C., Johnson, B.D.: Nebular Continuum and Line Emission in Stellar Population Synthesis Models. *ApJ* **840**(1), 44 (2017) <https://doi.org/10.3847/1538-4357/aa6c66> arXiv:1611.08305 [astro-ph.GA]

- [71] Chabrier, G.: Galactic Stellar and Substellar Initial Mass Function. *PASP* **115**(809), 763–795 (2003) <https://doi.org/10.1086/376392> arXiv:astro-ph/0304382 [astro-ph]
- [72] Bruzual, G., Charlot, S.: Stellar population synthesis at the resolution of 2003. *MNRAS* **344**(4), 1000–1028 (2003) <https://doi.org/10.1046/j.1365-8711.2003.06897.x> arXiv:astro-ph/0309134 [astro-ph]
- [73] Kroupa, P.: On the variation of the initial mass function. *MNRAS* **322**(2), 231–246 (2001) <https://doi.org/10.1046/j.1365-8711.2001.04022.x> arXiv:astro-ph/0009005 [astro-ph]
- [74] Charlot, S., Fall, S.M.: A Simple Model for the Absorption of Starlight by Dust in Galaxies. *ApJ* **539**(2), 718–731 (2000) <https://doi.org/10.1086/309250> arXiv:astro-ph/0003128 [astro-ph]
- [75] Leja, J., Carnall, A.C., Johnson, B.D., Conroy, C., Speagle, J.S.: How to Measure Galaxy Star Formation Histories. II. Nonparametric Models. *ApJ* **876**(1), 3 (2019) <https://doi.org/10.3847/1538-4357/ab133c> arXiv:1811.03637 [astro-ph.GA]
- [76] Vanden Berk, D.E., Richards, G.T., Bauer, A., Strauss, M.A., Schneider, D.P., Heckman, T.M., York, D.G., Hall, P.B., Fan, X., Knapp, G.R., Anderson, S.F., Annis, J., Bahcall, N.A., Bernardi, M., Briggs, J.W., Brinkmann, J., Brunner, R., Burles, S., Carey, L., Castander, F.J., Connolly, A.J., Crocker, J.H., Csabai, I., Doi, M., Finkbeiner, D., Friedman, S., Frieman, J.A., Fukugita, M., Gunn, J.E., Hennessy, G.S., Ivezić, Ž., Kent, S., Kunszt, P.Z., Lamb, D.Q., Leger, R.F., Long, D.C., Loveday, J., Lupton, R.H., Meiksin, A., Merelli, A., Munn, J.A., Newberg, H.J., Newcomb, M., Nichol, R.C., Owen, R., Pier, J.R., Pope, A., Rockosi, C.M., Schlegel, D.J., Siegmund, W.A., Smee, S., Snir, Y., Stoughton, C., Stubbs, C., SubbaRao, M., Szalay, A.S., Szokoly, G.P., Tremonti, C., Uomoto, A., Waddell, P., Yanny, B., Zheng, W.: Composite Quasar Spectra from the Sloan Digital Sky Survey. *AJ* **122**(2), 549–564 (2001) <https://doi.org/10.1086/321167> arXiv:astro-ph/0105231 [astro-ph]
- [77] Saccheo, I., Bongiorno, A., Piconcelli, E., Testa, V., Bischetti, M., Bisogni, S., Bruni, G., Cresci, G., Feruglio, C., Fiore, F., Grazian, A., Luminari, A., Lusso, E., Mainieri, V., Maiolino, R., Marconi, A., Ricci, F., Tombesi, F., Travascio, A., Vietri, G., Vignali, C., Zappacosta, L., La Franca, F.: The WISSH quasars project. XI. The mean spectral energy distribution and bolometric corrections of the most luminous quasars. *A&A* **671**, 34 (2023) <https://doi.org/10.1051/0004-6361/202244296> arXiv:2211.07677 [astro-ph.GA]
- [78] Bezanson, R., van der Wel, A., Straatman, C., Pacifici, C., Wu, P.-F., Barišić, I., Bell, E.F., Conroy, C., D’Eugenio, F., Franx, M., Gallazzi, A., van Houdt, J., Maseda, M.V., Muzzin, A., van de Sande, J., Sobral, D., Spilker, J.: 1D Kinematics from Stars and Ionized Gas at $z \sim 0.8$ from the LEGA-C Spectroscopic Survey of Massive Galaxies. *ApJ* **868**(2), 36 (2018) <https://doi.org/10.3847/2041-8213/>

aaf16b arXiv:1811.07900 [astro-ph.GA]

- [79] van der Wel, A., van Houdt, J., Bezanson, R., Franx, M., D'Eugenio, F., Straatman, C., Bell, E.F., Muzzin, A., Sobral, D., Maseda, M.V., de Graaff, A., Holden, B.P.: The Mass Scale of High-redshift Galaxies: Virial Mass Estimates Calibrated with Stellar Dynamical Models from LEGA-C. *ApJ* **936**(1), 9 (2022) <https://doi.org/10.3847/1538-4357/ac83c5> arXiv:2208.12605 [astro-ph.GA]
- [80] Tacconi, L.J., Genzel, R., Sternberg, A.: The Evolution of the Star-Forming Interstellar Medium Across Cosmic Time. *ARA&A* **58**, 157–203 (2020) <https://doi.org/10.1146/annurev-astro-082812-141034> arXiv:2003.06245 [astro-ph.GA]
- [81] Weinberger, R., Springel, V., Pakmor, R.: The AREPO Public Code Release. *ApJS* **248**(2), 32 (2020) <https://doi.org/10.3847/1538-4365/ab908c> arXiv:1909.04667 [astro-ph.IM]
- [82] Vogelsberger, M., Genel, S., Springel, V., Torrey, P., Sijacki, D., Xu, D., Snyder, G., Nelson, D., Hernquist, L.: Introducing the Illustris Project: simulating the coevolution of dark and visible matter in the Universe. *MNRAS* **444**(2), 1518–1547 (2014)
- [83] Springel, V., White, S.D.M., Jenkins, A., Frenk, C.S., Yoshida, N., Gao, L., Navarro, J., Thacker, R., Croton, D., Helly, J., Peacock, J.A., Cole, S., Thomas, P., Couchman, H., Evrard, A., Colberg, J., Pearce, F.: Simulations of the formation, evolution and clustering of galaxies and quasars. *Nature* **435**(7042), 629–636 (2005) <https://doi.org/10.1038/nature03597> arXiv:astro-ph/0504097 [astro-ph]